SIAM J. APPL. MATH.
Vol. 80, No. 4, pp. 1654–1677

SHARP-INTERFACE MODEL FOR SIMULATING SOLID-STATE DEWETTING IN THREE DIMENSIONS*

WEI JIANG†, QUAN ZHAO‡, AND WEIZHU BAO§

Abstract. The problem of simulating solid-state dewetting of thin films in three dimensions (3D) by using a sharp-interface approach is considered in this paper. Based on the thermodynamic variation, a speed method is used for calculating the first variation to the total surface energy functional. The speed method shares more advantages than the traditional use of parameterized curves (or surfaces); e.g., it is more intrinsic, and its variational structure (related with the Cahn–Hoffman $\boldsymbol{\xi}$-vector) is clearer. By making use of the first variation, necessary conditions for the equilibrium shape of the solid-state dewetting problem are given, and a kinetic sharp-interface model which includes the surface energy anisotropy is also proposed. This sharp-interface model describes the interface evolution in 3D which occurs through surface diffusion and contact line migration. By solving the proposed model, we perform numerical simulations to investigate the evolution of patterned films, e.g., the evolution of a cuboid and pinch-off of a long cuboid. Numerical simulations in 3D demonstrate the performance of the sharp-interface approach to capture many of the complexities observed in solid-state dewetting experiments.

Key words. solid-state dewetting, surface diffusion, Cahn–Hoffman $\boldsymbol{\xi}$-vector, thermodynamic variation, surface energy anisotropy, shape derivative

AMS subject classifications. 74G65, 74G15, 74H15, 49Q10

DOI. 10.1137/19M1251345

1. Introduction.

Driven by capillarity effects, solid thin films sitting on a substrate are rarely stable and could exhibit complex morphological changes, e.g., faceting [23, 53], edge retraction [51, 12, 55, 27], pinch-off [18, 26], fingering instabilities [25], and so on. This phenomenon, known as solid-state dewetting [46], has been widely observed in many thin film/substrate systems [23, 27]. On one hand, solid-state dewetting can be deleterious by fabricating the thin film structures, e.g., microelectronic and optoelectronic devices, thus destroying the reliability of the devices; on the other hand, it is advantageous and can be positively used to produce the well-controlled formation of an array of micro-/nanoscale particles, e.g., used in sensors [3] and as catalysts for carbon [37] and semiconductor nanowire growth [39]. Recently, solid-state dewetting has attracted considerable interest and has been widely studied by many experimental (e.g., [2, 33, 29, 36]) and theoretical (e.g., [5, 6, 15, 18, 22, 43, 48, 51]) research groups. The understanding of its equilibrium patterns and kinetic morphology evolution characteristics could provide important knowledge for developing new experimental methods in order to control solid-state dewetting [30] and enhance its potential applications in thin film technolo-

*Received by the editors March 20, 2019; accepted for publication (in revised form) April 13, 2020; published electronically July 16, 2020.
https://doi.org/10.1137/19M1251345
Funding: The work of the first author was supported by the NSFC through grant 11871384 and by the NSF of the Hubei Province through grant 2018CFB466. The work of the third author was supported by the NSFC through grant 91630207. The work of the second and third authors was supported by the Ministry of Education through grant R-146-000-247-114.

†School of Mathematics and Statistics & Hubei Key Laboratory of Computational Science, Wuhan University, Wuhan 430072, People's Republic of China (jiangwei1007@whu.edu.cn).
‡Corresponding author. Department of Mathematics, National University of Singapore, Singapore 119076 (quanzhao90@u.nus.edu).
§Department of Mathematics, National University of Singapore, Singapore 119076 (matbaowz@nus.edu.sg, http://www.blog.nus.edu.sg/matbaowz/).

gies.

Modeling solid-state dewetting has been an active research area and has become increasingly urgent in recent decades. In general, surface diffusion and contact line migration have been recognized as the two main kinetic features for the evolution of solid-state dewetting [5, 21]. In 1986, Srolovitz and Safran [43] proposed a simplified sharp-interface model to study the hole growth during the dewetting under the three assumptions, i.e., isotropic surface energy, small slope profile, and cylindrical symmetry. Based on the above model, Wong and his coworkers designed a "marker particle" numerical scheme to investigate the two-dimensional retraction of a discontinuous film (a film with a step) and the evolution of a perturbed cylindrical wire on a substrate [51, 13]. These earlier studies were focused on the isotropic surface energy, although recent experiments have demonstrated that the crystalline anisotropy could play important roles in solid-state dewetting. To include the surface energy anisotropy, many approaches have been proposed in recent years, such as a discrete model [12], a kinetic Monte Carlo model [35], a crystalline model [9, 59], and continuum models based on partial differential equations [6, 20, 21, 48]. From a mathematical perspective, theoretical solid-state dewetting studies can be categorized into two major problems: one focuses on the equilibrium of solid particles on substrates [5, 28]; the other focuses on investigating the kinetic evolution of solid-state dewetting [20, 21, 48]. In this paper, we aim at developing a sharp-interface model for studying these problems about solid-state dewetting in three dimensions (3D).

Under isothermal conditions, the equilibrium shape for a free-standing solid particle can be formulated by minimizing the interfacial energy subject to the constraint of a constant volume:

$$\min_{\Omega} W := W(S) = \int_S \gamma(\mathbf{n})\, dS \quad \text{s.t.} \quad |\Omega| = \text{const}, \tag{1.1}$$

where $\Omega \subset \mathbb{R}^3$ is the enclosed domain by a closed surface S, and $\gamma(\mathbf{n})$ is the surface energy (density) with $\mathbf{n} = (n_1, n_2, n_3)^T$ representing the crystallographic orientation. Based on the γ-plot, the equilibrium shape can be geometrically constructed via the well-known Wulff (Gibbs–Wulff) construction [52]. The resulting Wulff shape is the inner convex region bounded by all planes that are perpendicular to orientation $\mathbf{n}$ and at a distance of $\gamma(\mathbf{n})$ from the origin. The Wulff–Kaischew construction (also called the Winterbottom construction) [24, 50, 5] was subsequently proposed to handle the case about particles on substrates by truncating the Wulff shape with a flat plane, and where the Wulff shape is truncated depends on the wettability of the substrate. Meanwhile, many theories [7, 8] demonstrated that the derivative of $\gamma(\mathbf{n})$ plays an important role in investigating equilibrium and kinetic problems for solid particles with anisotropic surface energies. In 1972, Cahn and Hoffman developed the theory of $\boldsymbol{\xi}$-vector [17, 7] to describe the surface energy anisotropy of solid materials. It is defined based on a homogeneous extension of $\gamma(\mathbf{n})$, i.e.,

$$\boldsymbol{\xi}(\mathbf{n}) = \nabla\hat{\gamma}(\mathbf{p})\Big|_{\mathbf{p}=\mathbf{n}}, \text{ with } \hat{\gamma}(\mathbf{p}) = |\mathbf{p}|\gamma\left(\frac{\mathbf{p}}{|\mathbf{p}|}\right) \quad \forall \mathbf{p} \in \mathbb{R}^3\backslash\{\mathbf{0}\}, \tag{1.2}$$

where $|\mathbf{p}| := \sqrt{p_1^2 + p_2^2 + p_3^2}$ for $\mathbf{p} = (p_1, p_2, p_3)^T \in \mathbb{R}^3$. Under this extension, $\hat{\gamma}(\mathbf{p})$ satisfies

$$\hat{\gamma}(\lambda\mathbf{p}) = |\lambda|\hat{\gamma}(\mathbf{p}), \qquad \nabla\hat{\gamma}(\mathbf{p}) \cdot \mathbf{p} = \hat{\gamma}(\mathbf{p}) \quad \forall \lambda \neq 0, \mathbf{p} \in \mathbb{R}^3\backslash\{\mathbf{0}\}. \tag{1.3}$$

Compared to the traditional use of scalar function γ (or γ-plot), $\boldsymbol{\xi}$-vector formulation has some advantages in the description of equilibrium shapes and thermodynamic

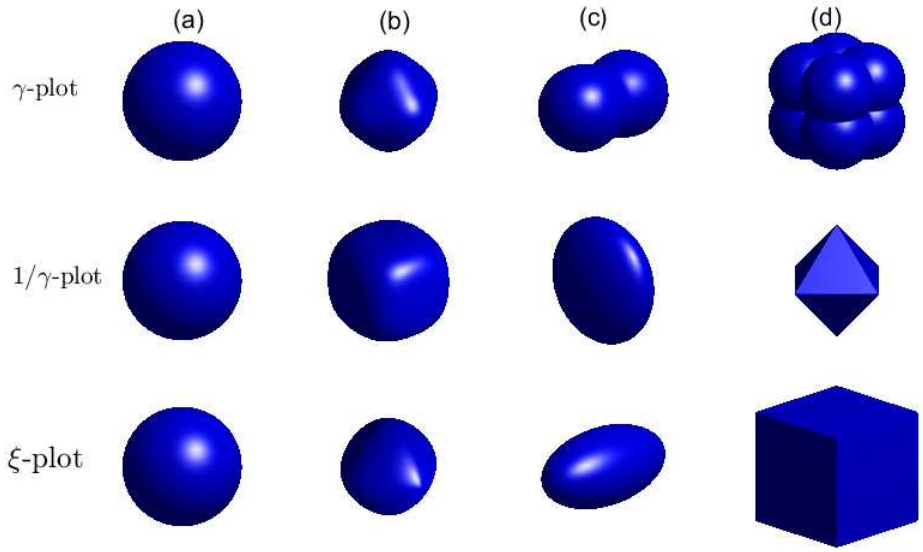

FIG. 1.1. *The γ-plot, $1/\gamma$-plot, and $\boldsymbol{\xi}$-plot for different surface energy anisotropies:* (a) *isotropic surface energy;* (b) *cubic anisotropic surface energy defined as* $\gamma(\mathbf{n}) = 1 + 0.3(n_1^4 + n_2^4 + n_3^4)$*;* (c) *ellipsoidal surface energy* $\gamma(\mathbf{n}) = \sqrt{4n_1^2 + n_2^2 + n_3^2}$*;* (d) *"cusped" surface energy defined as* $\gamma(\mathbf{n}) = |n_1| + |n_2| + |n_3|$.

evolution for crystalline interfaces [21, 49]. From (1.3), we have $\boldsymbol{\xi}(\mathbf{n}) \cdot \mathbf{n} = \gamma(\mathbf{n})$, and the magnitude of the normal component for $\boldsymbol{\xi}(\mathbf{n})$ equals $\gamma(\mathbf{n})$. Meanwhile, the $\boldsymbol{\xi}$-plot shares similar geometry with the Wulff shape, and it can be regarded as a mathematical representation of the equilibrium shape [7, 34, 40] when its $1/\gamma$-plot is convex (i.e., weakly anisotropic). Figure 1.1 depicts the γ-plot, $1/\gamma$-plot, and $\boldsymbol{\xi}$-plot for four different types of surface energy anisotropies: (a) isotropic surface energy, i.e., $\gamma(\mathbf{n}) \equiv 1$; (b) cubic surface energy $\gamma(\mathbf{n}) = 1 + a(n_1^4 + n_2^4 + n_3^4)$, with a representing the degree of anisotropy; (c) ellipsoidal surface energy $\gamma(\mathbf{n}) = \sqrt{a_1^2 n_1^2 + a_2^2 n_2^2 + a_3^2 n_3^2}$; (d) "cusped" surface energy defined as $\gamma(\mathbf{n}) = |n_1| + |n_2| + |n_3|$. In the application of materials science, the surface energy could be piecewise smooth and have some "cusped" points, where it is not differentiable [6, 34]. A typical example is the "cusped" surface energy defined above. For these cases, we can regularize the surface energy with a small parameter $0 < \varepsilon \ll 1$ to ensure the usage of the sharp-interface approach proposed in this paper, i.e.,

$$\gamma(\mathbf{n}) = \sqrt{\varepsilon^2 + (1-\varepsilon^2)n_1^2} + \sqrt{\varepsilon^2 + (1-\varepsilon^2)n_2^2} + \sqrt{\varepsilon^2 + (1-\varepsilon^2)n_3^2}. \tag{1.4}$$

Note that ε is used to smooth the surface energy, and it could relate with the width (or scale) of the rounded corner in nanoparticles [1, 6].

The Cahn–Hoffman $\boldsymbol{\xi}$-vector has been recently utilized to describe the solid-state dewetting problem in two dimensions (2D) [21]. Based on the thermodynamic variation, the authors derived a sharp-interface approach via the $\boldsymbol{\xi}$-vector formulation for describing the kinetic evolution of solid-state dewetting in 2D. In this approach, the moving interface is described as a parameterization over a time-independent domain, and the variation is performed by considering an infinitesimal perturbation with respect to an open interface curve coupled with contact points [21]. However,

when we want to generalize this approach to 3D, we realize that it would be very different for calculating the thermodynamic variation for the three-dimensional problem by using the approach of parameterized surfaces. First, the calculations of the variation in 3D via a surface parameterization approach would become complicated, extremely tedious, and a nightmare, and it unavoidably involves a lot of knowledge about differential geometry. Second, for the solid-state dewetting problem, the infinitesimal perturbation to a surface in the tangential direction plays an important role in investigating the contact line migration along the substrate [20, 5], and it would make the calculations become more complicated. Third, complicated calculations often make people easily forget the nature of the problem, and we need to investigate and make use of the variational structure of the problem. These difficulties motivate us to look for a new approach to calculating the thermodynamic variation of solid-state dewetting in 3D. In the literature, the shape optimization problem is popular in the design of industrial structures. The speed method and shape derivatives have been widely utilized to perform the shape sensitivity analysis of shape optimization problems [41, 16, 11]. This approach avoids the parameterization of a surface and is able to deal with perturbations along arbitrary directions, and it is the desired tool for which we are searching.

Therefore, based on the $\boldsymbol{\xi}$-vector formulation and the speed method, the objectives of this paper are as follows: (i) to calculate the thermodynamic variation of the energy functional for solid-state dewetting in 3D; (ii) to provide a rigorous derivation of the thermodynamic description of the equilibrium shape for solid-state dewetting in 3D; (iii) to develop a sharp-interface model which includes surface diffusion and contact line migration for simulating kinetic evolution of solid-state dewetting in 3D; and (iv) to present numerical simulations to investigate important characteristics of the morphological evolution for solid-state dewetting observed in experiments.

The rest of the paper is organized as follows. In section 2, we briefly introduce the speed method and sharp derivatives and then apply them for calculating the first variation of the total free energy functional. In section 3, we rigorously derive the necessary conditions for the equilibrium shape and explicitly give an expression for the equilibrium shape by using a parametric formula. In section 4, based on thermodynamic variation, a sharp-interface model is proposed for simulating solid-state dewetting of thin films in 3D. Subsequently, we perform some numerical simulations to demonstrate the performance of our proposed model in section 5. Finally, we draw some conclusions in section 6.

2. Thermodynamic variation. The solid-state dewetting problem can be illustrated as Figure 2.1, where a solid thin film (in blue) can dewet or agglomerate on a flat rigid substrate (in gray) due to capillarity effects. The total interfacial free energy of the system can be written as [5, 21]

$$W = \int_{S_{FV}} \gamma_{FV}\, dS_{FV} + \underbrace{\int_{S_{FS}} \gamma_{FS}\, dS_{FS} + \int_{S_{VS}} \gamma_{VS}\, dS_{VS}}_{\text{Substrate energy}},$$

where $S_{FV} := S$, S_{FS}, and S_{VS} represent the film/vapor, film/substrate, and vapor/substrate interfaces, respectively, and γ_{FV}, γ_{FS}, and γ_{VS} represent the corresponding surface energy densities. In solid-state dewetting problems, we often assume that γ_{FS}, γ_{VS} are two constants, and γ_{FV} is a function of the orientation of the film/vapor interface, i.e., $\gamma_{FV} := \gamma(\mathbf{n})$, with $\mathbf{n}$ representing the unit normal vector of

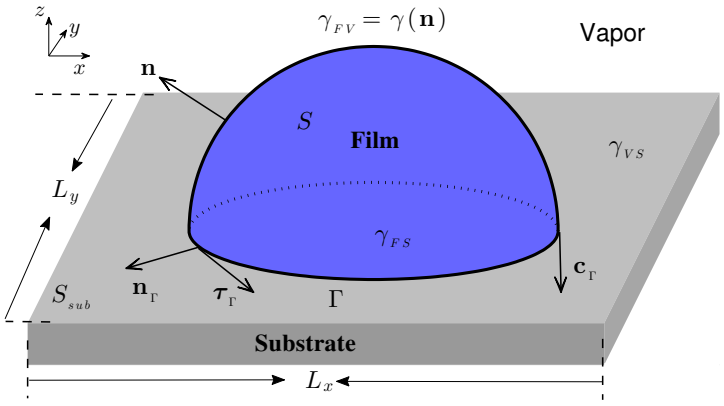

FIG. 2.1. *A schematic illustration of the solid-state dewetting of a solid thin film (in blue) on a flat, rigid substrate (in gray) in 3D.*

the film/vapor interface, which points outwards to the vapor phase. The film/vapor interface is here described by an open two-dimensional surface S with boundary Γ (i.e., the contact line), which is a closed plane curve on the flat substrate S_{sub}.

Assume that we consider a bounded domain with size $L_x \times L_y$ on the substrate (shown in Figure 2.1). If we label the surface area enclosed by the contact line Γ as $A(\Gamma)$, then the total interfacial free energy of the system can be calculated as

$$\begin{aligned} W &= \int_{S_{FV}} \gamma_{FV}\, dS_{FV} + \int_{S_{FS}} \gamma_{FS}\, dS_{FS} + \int_{S_{VS}} \gamma_{VS}\, dS_{VS} \\ &= \int_S \gamma(\mathbf{n})\, dS + (\gamma_{FS} - \gamma_{VS})A(\Gamma) + L_x\, L_y\, \gamma_{VS}. \end{aligned}$$

By dropping off the constant term $L_x L_y \gamma_{VS}$, we can simplify the total interfacial free energy (still labeled as W) as the following two parts, i.e., the film/vapor interface energy term W_{int} and the substrate energy term W_{sub}:

$$W = W_{\text{int}} + W_{\text{sub}} = \int_S \gamma(\mathbf{n})\, dS + (\gamma_{FS} - \gamma_{VS})A(\Gamma). \tag{2.1}$$

As shown in Figure 2.1, we introduce three unit vectors $\mathbf{n}_\Gamma$, $\boldsymbol{\tau}_\Gamma$, and $\mathbf{c}_\Gamma$, which are defined along the boundary Γ. More precisely, $\mathbf{n}_\Gamma$ is the outer unit normal vector of the plane curve Γ on the substrate S_{sub}; $\boldsymbol{\tau}_\Gamma$ is the unit tangent vector of Γ on the substrate S_{sub}, which points counterclockwise when looking from top to bottom; and $\mathbf{c}_\Gamma$ is called the conormal vector, which is normal to Γ and tangent to the surface S and points downwards. For any point $\mathbf{x} \in S$ (with $\mathbf{x} = (x_1, x_2, x_3)^T$ or $(x, y, z)^T$), if we label $\mathcal{T}_{\mathbf{x}} S$ as the tangent vector space to S at $\mathbf{x}$, then the following properties are valid:

$$\begin{aligned} &\boldsymbol{\tau}_\Gamma(\mathbf{x}) \in \mathcal{T}_{\mathbf{x}} S, \quad && \boldsymbol{\tau}_\Gamma(\mathbf{x}) \parallel S_{\text{sub}}, \quad && \boldsymbol{\tau}_\Gamma(\mathbf{x}) \perp \mathbf{c}_\Gamma(\mathbf{x}) \quad \forall \mathbf{x} \in \Gamma, \\ &\mathbf{c}_\Gamma(\mathbf{x}) \in \mathcal{T}_{\mathbf{x}} S, \quad && \mathbf{n}_\Gamma(\mathbf{x}) \parallel S_{\text{sub}}, \quad && \mathbf{n}_\Gamma(\mathbf{x}) \perp \boldsymbol{\tau}_\Gamma(\mathbf{x}) \quad \forall \mathbf{x} \in \Gamma. \end{aligned}$$

2.1. Differential operators on manifolds. To obtain the first variation of the above shape functional (2.1), we start by introducing some basic knowledge about surface calculus. For more details, readers can refer to [14, 10].

DEFINITION 2.1. *Suppose that $S \subset \mathbb{R}^3$ is a two-dimensional smooth manifold, and suppose that a function f is defined on S such that $f \in C^2(S)$. Let $\mathbf{n} = (n_1,\ n_2,\ n_3)^T$ be the unit outer normal vector of S, and let $\bar{f}$ be an extension of f in the neighborhood of S such that $\bar{f}$ is differentiable; then the surface gradient of f on S is defined as*

$$\nabla_{_S} f = \nabla \bar{f} - (\nabla \bar{f} \cdot \mathbf{n})\, \mathbf{n}, \tag{2.2}$$

with ∇ denoting the usual gradient in $\mathbb{R}^3$. It is easy to show that $\nabla_{_S} f$ is independent of the extension of f and only dependent on the value of f on S. If we denote $\nabla_{_S}$ as a vector operator

$$\nabla_{_S} = (\underline{D}_1,\ \underline{D}_2,\ \underline{D}_3)^T, \tag{2.3}$$

then we can easily obtain

$$\underline{D}_i x_j = \delta_{ij} - n_i\, n_j \qquad \forall 1 \le i,\, j \le 3, \tag{2.4}$$

where $\mathbf{x} = (x_1, x_2, x_3)$ is the position vector of the surface and δ_{ij} is the Kronecker delta. The surface divergence of a vector-valued function $\mathbf{g} = (g_1,\ g_2,\ g_3)^T \in [C^1(S)]^3$ is defined as

$$\nabla_{_S} \cdot \mathbf{g} = \sum_{i=1}^{3} \underline{D}_i\, g_i. \tag{2.5}$$

Moreover, the Laplace–Beltrami operator on S can be expressed as

$$\Delta_{_S}\, f = \nabla_{_S} \cdot (\nabla_{_S}\, f) = \sum_{i=1}^{3} \underline{D}_i \underline{D}_i f. \tag{2.6}$$

In the definition of surface gradient, since the normal component has been subtracted from $\nabla \bar{f}$, $\nabla_{_S} f$ can be viewed as the tangential component of $\nabla \bar{f}$, and thus we have $\nabla_{_S} f \cdot \mathbf{n} = 0$ and $\nabla_{_S} f(\mathbf{x}) \in \mathcal{T}_{\mathbf{x}} S$ for all $\mathbf{x} \in S$. Note that it can be rigorously proved that Definition 2.1 is consistent with the conventional definition in differential geometry [14], and it generalizes the definition domain of surface divergence from the vector in tangent vector spaces to any vector in $\mathbb{R}^3$.

On the other hand, the integration by parts on an open smooth surface S with smooth boundary Γ reads as (see Theorem 2.10 in [14], and we omit the proof here)

$$\int_S \nabla_{_S} f\ dS = \int_S f\, \mathcal{H}\, \mathbf{n}\ dS + \int_\Gamma f\, \mathbf{c}_{_\Gamma}\ d\Gamma, \tag{2.7}$$

where $\mathbf{n}$ and $\mathbf{c}_{_\Gamma}$ are the normal and conormal vectors (shown in Figure 2.1), respectively, and $\mathcal{H}$ is the mean curvature, which is defined as the surface divergence of the unit normal vector, i.e., $\mathcal{H} = \nabla_{_S} \cdot \mathbf{n}$. Similarly, by using the above equation and Definition 2.1, we can obtain the integration by parts about a vector field $\mathbf{F} = (f_1, f_2, f_3)^T \in \mathbb{R}^3$ defined on an open smooth surface S with smooth boundary Γ,

$$\int_S \nabla_{_S} \cdot \mathbf{F}\ dS = \int_S \mathcal{H}\, \mathbf{F} \cdot \mathbf{n}\ dS + \int_\Gamma \mathbf{F} \cdot \mathbf{c}_{_\Gamma}\ d\Gamma. \tag{2.8}$$

If $\mathbf{F}$ lies in the tangent vector space of S, i.e., $\mathbf{F} \cdot \mathbf{n} = 0$, then the first term on the right-hand side will vanish.

Furthermore, by using the product rule that $\nabla_S(fg) = g\,\nabla_S f + f\,\nabla_S g$, we can obtain

$$\int_S g\,\nabla_S f\,dS = -\int_S f\,\nabla_S g\,dS + \int_S f\,g\,\mathcal{H}\,\mathbf{n}\,dS + \int_\Gamma f\,g\,\mathbf{c}_\Gamma\,d\Gamma. \tag{2.9}$$

In a simple case, if S is a flat surface (i.e., $\mathcal{H} = 0$) with a plane boundary curve Γ, then (2.7) reduces to

$$\int_S \nabla_S f\,dS = \int_\Gamma f\,\mathbf{c}_\Gamma\,d\Gamma,$$

which is the Gauss–Green theorem in the multivariable calculus, because $\nabla_S f$ collapses to the gradient of f in 2D, and $\mathbf{c}_\Gamma$ collapses to the unit outer normal vector of Γ.

2.2. The speed method and shape derivative. In this section, the objective is to calculate the first variation of the energy (or shape) functional defined in (2.1). To this end, we first introduce an independent parameter $\epsilon \in [0, \epsilon_0)$ to parameterize a family of perturbations of a given domain $D \subset \mathbb{R}^3$, where the parameter ϵ controls the amplitude of the perturbation and ϵ_0 is the maximum perturbation amplitude. Furthermore, we assume that the domain D is of class C^k, with $k \geq 2$.

More precisely, we consider a domain $D \subset \mathbb{R}^3$ with a piecewise smooth boundary ∂D; then we can construct a family of transformations T_ϵ, which are one-to-one, and T_ϵ maps from $\bar{D}$ onto $\bar{D}$, i.e.,

$$T_\epsilon :\ \bar{D}\ \rightarrow\ \bar{D}, \qquad \epsilon \in [0, \epsilon_0), \tag{2.10}$$

where ϵ is the small perturbation parameter. Generally, we assume that (i) T_ϵ and T_ϵ^{-1} belong to $C^k(\bar{D}, \mathbb{R}^3)$ for all $\epsilon \in [0, \epsilon_0)$, with $k \geq 2$; and (ii) the mappings $\epsilon \rightarrow T_\epsilon(\mathbf{x})$ and $\epsilon \rightarrow T_\epsilon^{-1}(\mathbf{x})$ belong to $C^1[0, \epsilon_0)$ for all $\mathbf{x} \in \mathbb{R}^3$ (with $\mathbf{x} = (x_1, x_2, x_3)^T$).

Given any point $\mathbf{X} \in \bar{D}$ (with $\mathbf{X} = (X_1, X_2, X_3)^T$) and $\epsilon \in [0, \epsilon_0)$, we can define the point $\mathbf{x} = T_\epsilon(\mathbf{X})$ which moves along the trajectory. Here, the point $\mathbf{X}$ represents the Lagrangian (or material) coordinate, while $\mathbf{x}$ is the Eulerian (or actual) coordinate. Therefore, the speed vector field $\mathbf{V}(\mathbf{x}, \epsilon)$ at point $\mathbf{x}$ is defined as

$$\mathbf{V}(\mathbf{x}, \epsilon) = \frac{\partial \mathbf{x}}{\partial \epsilon}(T_\epsilon^{-1}(\mathbf{x}), \epsilon). \tag{2.11}$$

On the other hand, the transformation T_ϵ can be uniquely determined by the speed vector field $\mathbf{V}$ via the following ordinary differential equation:

$$\begin{cases} \frac{d}{d\epsilon}\mathbf{x}(\mathbf{X}, \epsilon) = \mathbf{V}(\mathbf{x}(\mathbf{X}, \epsilon), \epsilon), \\ \mathbf{x}(\mathbf{X}, 0) = \mathbf{X}. \end{cases} \tag{2.12}$$

Therefore, the transformation T_ϵ and the smooth vector field $\mathbf{V}$ are uniquely determined by each other. For a smooth vector field $\mathbf{V}$, e.g., $\mathbf{V} \in C(C^k(\bar{D}, \mathbb{R}^3); [0, \epsilon_0))$, the equivalence between the transformation T_ϵ and the speed vector field $\mathbf{V}$ has been strictly established by Theorem 2.16 in [41]. In the following, we use $T_\epsilon(\mathbf{V})$ to denote the transformation associated with vector field $\mathbf{V}$. For simplicity, we also denote $\mathbf{V}_0 = \mathbf{V}(\mathbf{X}, 0)$.

Let $J(G)$ be a shape functional defined on a shape $G \subset \bar{D}$, where G could be a three-dimensional domain (e.g., Ω) or a two-dimensional manifold (e.g., a surface S).

The first variation of the functional $J(G)$ at G in the direction of a speed vector field $\mathbf{V} \in C(C^k(\bar{D}, \bar{D}); [0, \epsilon_0))$ is given as the Eulerian derivative:

$$\delta J(G; \mathbf{V}) = \lim_{\epsilon \to 0} \frac{J(G_\epsilon) - J(G)}{\epsilon}, \tag{2.13}$$

where $G_\epsilon = T_\epsilon(\mathbf{V})(G)$. Based on the transformation, in order to obtain the first variation, we first define the material derivative and shape derivative of a function on a domain Ω or a surface S. For more details about the shape differential calculus, we refer readers to the book by Sokołowski and Zolesio [41].

DEFINITION 2.2 (material derivatives; Definitions 2.71 and 2.74 in [41]). *The material derivative $\dot{\psi}(\Omega; \mathbf{V})$ of ψ* on a domain Ω *in the direction of a speed vector field $\mathbf{V}$ is defined as*

$$\dot{\psi}(\Omega; \mathbf{V}) = \lim_{\epsilon \to 0} \frac{\psi(\Omega_\epsilon) \circ T_\epsilon(\mathbf{V}) - \psi(\Omega)}{\epsilon}, \tag{2.14}$$

where for $\mathbf{X} \in \Omega$, $\psi(\Omega_\epsilon) \circ T_\epsilon(\mathbf{V}) = \psi(T_\epsilon(\mathbf{X}))$.

Similarly, the material derivative $\dot{\varphi}(S; \mathbf{V})$ of φ on a surface S *in the direction $\mathbf{V}$ is defined as*

$$\dot{\varphi}(S; \mathbf{V}) = \lim_{\epsilon \to 0} \frac{\varphi(S_\epsilon) \circ T_\epsilon(\mathbf{V}) - \varphi(S)}{\epsilon}, \tag{2.15}$$

where for $\mathbf{X} \in S$, $\varphi(S_\epsilon) \circ T_\epsilon(\mathbf{V}) = \varphi(T_\epsilon(\mathbf{X}))$.

DEFINITION 2.3 (shape derivatives; Definitions 2.85 and 2.88 in [41]). *The shape derivative $\psi'(\Omega; \mathbf{V})$ of ψ defined* on a domain Ω *in the direction $\mathbf{V}$ is defined as*

$$\psi'(\Omega; \mathbf{V}) = \dot{\psi}(\Omega; \mathbf{V}) - \nabla \psi(\Omega) \cdot \mathbf{V}_0. \tag{2.16}$$

Similarly, the shape derivative $\varphi'(S; \mathbf{V})$ of φ defined on a surface S *in the direction $\mathbf{V}$ is defined as*

$$\varphi'(S; \mathbf{V}) = \dot{\varphi}(S; \mathbf{V}) - \nabla_S \varphi(S) \cdot \mathbf{V}_0. \tag{2.17}$$

PROPOSITION 2.1. *Let $\Omega \subset \mathbb{R}^3$ be a smooth bounded domain in $\bar{D}$ with smooth boundary $\partial\Omega$, and let $\mathbf{V}$ be a speed vector field such that $\mathbf{V} \in C(C^k(\bar{D}, \bar{D}); [0, \epsilon_0))$. Suppose that $\psi = \psi(\Omega)$ is given such that the material derivative $\dot{\psi}(\Omega; \mathbf{V})$ and the shape derivative $\psi'(\Omega; \mathbf{V})$ exist. Then, the shape functional $J(\Omega) = \int_\Omega \psi(\Omega)\, d\Omega$ is shape differentiable and we have*

$$\delta J(\Omega; \mathbf{V}) = \int_\Omega \psi'(\Omega; \mathbf{V})\, d\Omega + \int_{\partial\Omega} \psi(\Omega)\, \mathbf{V}_0 \cdot \mathbf{n}\, d\Omega. \tag{2.18}$$

Proof. See section 2.31 on pages 112–113 in [41]. ∎

REMARK 2.1. *If $\mathbf{V}_0 \cdot \mathbf{n} = 0$ on the boundary $\partial\Omega$, we obtain that the first variation of the functional reduces to*

$$\delta J(\Omega; \mathbf{V}) = \int_\Omega \psi'(\Omega; \mathbf{V})\, d\Omega. \tag{2.19}$$

Furthermore, the definition of shape derivative for a function $\varphi(S)$ defined over a two-dimensional manifold S ensures that the shape derivative shows no dependence on the extension of φ in the near neighborhood. We propose the following proposition to show that the first variation of a functional on S is closely related to the shape derivative.

PROPOSITION 2.2. *Let S be a two-dimensional smooth manifold in $\bar{D}$ with smooth boundary Γ, and let $\mathbf{V}$ be a speed vector field such that $\mathbf{V} \in C(C^k(\bar{D}, \bar{D}); [0, \epsilon_0))$. Suppose that $\varphi = \varphi(S)$ is given such that the material derivative $\dot{\varphi}(S; \mathbf{V})$ and the shape derivative $\varphi'(S; \mathbf{V})$ exist. Then, the shape functional $J(S) = \int_S \varphi(S)\, dS$ is shape differentiable and we have*

$$\delta J(S; \mathbf{V}) = \int_S \varphi'(S; \mathbf{V})\, dS + \int_S \varphi(S)\mathcal{H}\mathbf{V}_0 \cdot \mathbf{n}\, dS + \int_\Gamma \varphi(S)\mathbf{V}_0 \cdot \mathbf{c}_\Gamma\, d\Gamma, \tag{2.20}$$

where $\mathcal{H}$ is the mean curvature of the surface S, and $\mathbf{c}_\Gamma$ is the unit conormal vector. Furthermore, if $\varphi(S) = \psi(\Omega)\Big|_S$, then we have

$$\delta J(S; \mathbf{V}) = \int_S \psi'(\Omega; \mathbf{V})\Big|_S\, dS + \int_S \left(\frac{\partial \psi}{\partial \mathbf{n}} + \psi\mathcal{H}\right)\mathbf{V}_0 \cdot \mathbf{n}\, dS + \int_\Gamma \psi \mathbf{V}_0 \cdot \mathbf{c}_\Gamma\, d\Gamma. \tag{2.21}$$

Proof. By referring to section 2.33 on pages 115–116 in [41], we can directly obtain

$$\delta J(S; \mathbf{V}) = \int_S \dot{\varphi}(S; \mathbf{V})\, dS + \int_S \varphi(S)\nabla_{_S} \cdot \mathbf{V}_0\, dS. \tag{2.22}$$

By using integration by parts and also making use of (2.17), we obtain

$$\begin{aligned}\delta J(S; \mathbf{V}) &= \int_S \dot{\varphi}(S; \mathbf{V}_0)\, dS - \int_S \nabla_{_S}\varphi(S) \cdot \mathbf{V}_0\, dS + \int_S \varphi(S)\mathcal{H}\mathbf{V}_0 \cdot \mathbf{n}\, dS \\ &\quad + \int_\Gamma \varphi(S)\mathbf{V}_0 \cdot \mathbf{c}_\Gamma\, d\Gamma \\ &= \int_S \varphi'(S; \mathbf{V})\, dS + \int_S \varphi(S)\mathcal{H}\mathbf{V}_0 \cdot \mathbf{n}\, dS + \int_\Gamma \varphi(S)\mathbf{V}_0 \cdot \mathbf{c}_\Gamma\, d\Gamma. \end{aligned} \tag{2.23}$$

Furthermore, notice that the definitions of shape derivatives on the domain Ω and the surface S are different (see (2.16)–(2.17)). If we assume that ψ is a function defined on the domain Ω, such that its restriction on S equals the function $\varphi(S)$, i.e., $\psi(\Omega)\Big|_S = \varphi(S)$, we can reformulate (2.23) in terms of the extension function $\psi(\Omega)$ as

$$\delta J(S; \mathbf{V}) = \int_S \psi'(\Omega; \mathbf{V})\Big|_S\, dS + \int_S \left(\frac{\partial \psi}{\partial \mathbf{n}} + \psi\mathcal{H}\right)\mathbf{V}_0 \cdot \mathbf{n}\, dS + \int_\Gamma \psi \mathbf{V}_0 \cdot \mathbf{c}_\Gamma\, d\Gamma,$$

which completes the proof. ∎

REMARK 2.2. *If S is a closed surface, then the boundary term about Γ in* (2.21) *will vanish. Similar results for a closed curve or surface can be found in* [11, 16].

In the following, we will apply (2.21) in Proposition 2.2 for calculating the first variation of the energy (or shape) functional defined in (2.1), where the integrand is the surface energy density $\gamma(\mathbf{n})$. To calculate the shape derivatives and obtain the first variation, we shall make use of the signed distance function, which is a powerful tool in shape sensitivity analysis. Consider a closed domain $\Omega \subset \mathbb{R}^3$ with a smooth boundary surface $\partial\Omega$, and then the signed distance function is defined as

$$b(\mathbf{x}) = \begin{cases} \operatorname{dist}(\mathbf{x}, \partial\Omega) & \forall \mathbf{x} \in \mathbb{R}^3 \backslash \Omega, \\ 0 & \forall \mathbf{x} \in \partial\Omega, \\ -\operatorname{dist}(\mathbf{x}, \partial\Omega) & \forall \mathbf{x} \in \Omega. \end{cases} \tag{2.24}$$

Here, $\operatorname{dist}(\mathbf{x},\partial\Omega)=\inf_{\mathbf{y}\in\partial\Omega}|\mathbf{x}-\mathbf{y}|$. The signed distance function $b(\mathbf{x})$ can be used to determine the unit outer normal vector $\mathbf{n}$ and the mean curvature $\mathcal{H}$ on the boundary surface $\partial\Omega$. More precisely, we can extend the functions $\mathbf{n}$ and $\mathcal{H}$ which are defined on $\partial\Omega$ in terms of $b(\mathbf{x})$ in a tubular neighborhood such that

$$\mathbf{n}(\mathbf{x})=\nabla b(\mathbf{x})\Big|_{\partial\Omega},\quad \mathcal{H}(\mathbf{x})=\Delta b(\mathbf{x})\Big|_{\partial\Omega}\quad \forall\mathbf{x}\in\partial\Omega. \tag{2.25}$$

The shape derivative of the signed distance function in the direction of a vector field $\mathbf{V}$ is calculated as $b'(\Omega;\mathbf{V})=-\mathbf{V}_0\cdot\mathbf{n}$ (see [11, 16] for more details). Moreover, based on the extension, the shape derivatives of the two extension functions restricted on $\partial\Omega$ are also obtained (see Lemma 3.1 in [11]), i.e.,

$$\mathbf{n}'(\Omega;\mathbf{V})\Big|_{\partial\Omega}=-\nabla_{\!S}(\mathbf{V}_0\cdot\mathbf{n}),\qquad \mathcal{H}'(\Omega;\mathbf{V})\Big|_{\partial\Omega}=-\Delta_S(\mathbf{V}_0\cdot\mathbf{n}). \tag{2.26}$$

2.3. First variation. By applying (2.21) and making use of the shape derivative of the unit outer normal vector, we obtain the following lemma.

LEMMA 2.1. *Assume that $S\subset\bar{D}$ is a two-dimensional smooth manifold with smooth boundary Γ. Let $\mathbf{n}$ be the unit outer normal vector of S, and let $\mathbf{V}$ be a speed vector field such that $\mathbf{V}\in C(C^k(\bar{D},\bar{D});[0,\epsilon_0))$. If the shape functional $J(S)=\int_S\gamma(\mathbf{n})\,dS$ with a surface energy (density) $\gamma(\mathbf{n})$, then the first variation of $J(S)$ is given as*

$$\delta J(S;\mathbf{V})=\int_S(\nabla_{\!S}\cdot\boldsymbol{\xi})\,(\mathbf{V}_0\cdot\mathbf{n})\,dS+\int_\Gamma\mathbf{V}_0\cdot\mathbf{c}_\Gamma^\gamma\,d\Gamma, \tag{2.27}$$

where $\boldsymbol{\xi}:=\boldsymbol{\xi}(\mathbf{n})$ is the Cahn–Hoffman vector, which was defined previously in (1.2)*, $\mathbf{V}_0\cdot\mathbf{n}$ represents the deformation velocity along the outer normal direction of the interface S, and the vector $\mathbf{c}_\Gamma^\gamma:=(\boldsymbol{\xi}\cdot\mathbf{n})\,\mathbf{c}_\Gamma-(\boldsymbol{\xi}\cdot\mathbf{c}_\Gamma)\,\mathbf{n}$ with $\mathbf{c}_\Gamma$ representing the unit conormal vector (shown in Figure* 2.1*).*

Proof. We first assume $\hat{\gamma}(\mathbf{p})$ is a homogeneous extension of $\gamma(\mathbf{n})$,

$$\hat{\gamma}(\mathbf{p})=|\mathbf{p}|\gamma\left(\frac{\mathbf{p}}{|\mathbf{p}|}\right)\qquad\forall\,\mathbf{p}\in\mathbb{R}^3\backslash\{\mathbf{0}\}, \tag{2.28}$$

where the definition domain of the function $\gamma(\mathbf{n})$ changes from unit vectors $\mathbf{n}$ to arbitrary nonzero vectors $\mathbf{p}\in\mathbb{R}^3$.

We next consider a bounded domain $\Omega\subset\mathbb{R}^3$ such that $S\subset\partial\Omega$. Then, based on the signed distance function defined in (2.24), we can define $\nabla b(\mathbf{x})\in\mathbb{R}^3$ as an extension of the normal vector $\mathbf{n}$ in the neighborhood of S. Thus we can reformulate

$$J(S)=\int_S\hat{\gamma}\big(\nabla b(\mathbf{x})\big)\Big|_S\,dS=\int_S\psi(\Omega)\Big|_S\,dS, \tag{2.29}$$

with $\psi(\Omega):=\hat{\gamma}\big(\nabla b(\mathbf{x})\big)$. Using the chain rule for shape derivatives and the definition of the Cahn–Hoffman $\boldsymbol{\xi}$-vector in (1.2), we conclude that the following expression holds:

$$\psi'(\Omega;\mathbf{V})\Big|_S=\nabla\hat{\gamma}\big(\nabla b(\mathbf{x})\big)\Big|_S\cdot\mathbf{n}'(\Omega;\mathbf{V})\Big|_S=-\boldsymbol{\xi}\cdot\nabla_{\!S}(\mathbf{V}_0\cdot\mathbf{n}). \tag{2.30}$$

Moreover, by noting the fact that $|\nabla b(\mathbf{x})|=1$, we obtain

$$\frac{\partial\psi}{\partial\mathbf{n}}\Big|_S=\boldsymbol{\xi}\cdot\big((\nabla\nabla b(\mathbf{x}))\;\nabla b(\mathbf{x})\big)\Big|_S=0, \tag{2.31}$$

where $\nabla\nabla b(\mathbf{x}) \in \mathbb{R}^{3\times 3}$. By making use of (2.21) and combining (2.30)–(2.31), we immediately have

$$\begin{aligned}\delta J(S;\mathbf{V}) &= -\int_S \boldsymbol{\xi}\cdot\nabla_S(\mathbf{V}_0\cdot\mathbf{n})\,dS + \int_S \gamma(\mathbf{n})\,(\mathbf{V}_0\cdot\mathbf{n})\,\mathcal{H}\,dS + \int_\Gamma \gamma(\mathbf{n})\,(\mathbf{V}_0\cdot\mathbf{c}_\Gamma)\,d\Gamma\\ &:= I + II + III.\end{aligned}$$

For the first term, by using the integration by parts, we obtain

$$I = \int_S (\nabla_S\cdot\boldsymbol{\xi})\,(\mathbf{V}_0\cdot\mathbf{n})\,dS - \int_S (\boldsymbol{\xi}\cdot\mathbf{n})\,(\mathbf{V}_0\cdot\mathbf{n})\,\mathcal{H}\,dS - \int_\Gamma (\boldsymbol{\xi}\cdot\mathbf{c}_\Gamma)\,(\mathbf{V}_0\cdot\mathbf{n})\,d\Gamma.$$

Based on (1.3), we have $\gamma(\mathbf{n}) = \boldsymbol{\xi}\cdot\mathbf{n}$. Thus we can rewrite

$$II = \int_S (\boldsymbol{\xi}\cdot\mathbf{n})\,(\mathbf{V}_0\cdot\mathbf{n})\mathcal{H}\,dS, \qquad III = \int_\Gamma (\boldsymbol{\xi}\cdot\mathbf{n})\,(\mathbf{V}_0\cdot\mathbf{c}_\Gamma)\,d\Gamma.$$

Finally, by combining the above three terms together, we immediately have

$$\begin{aligned}\delta J(S;\mathbf{V}) &= \int_S (\nabla_S\cdot\boldsymbol{\xi})\,(\mathbf{V}_0\cdot\mathbf{n})\,dS + \int_\Gamma \Big[(\boldsymbol{\xi}\cdot\mathbf{n})\,\mathbf{c}_\Gamma - (\boldsymbol{\xi}\cdot\mathbf{c}_\Gamma)\,\mathbf{n}\Big]\cdot\mathbf{V}_0\,d\Gamma\\ &= \int_S (\nabla_S\cdot\boldsymbol{\xi})\,(\mathbf{V}_0\cdot\mathbf{n})\,dS + \int_\Gamma \mathbf{c}_\Gamma^\gamma\cdot\mathbf{V}_0\,d\Gamma,\end{aligned}$$

where $\mathbf{c}_\Gamma^\gamma = (\boldsymbol{\xi}\cdot\mathbf{n})\,\mathbf{c}_\Gamma - (\boldsymbol{\xi}\cdot\mathbf{c}_\Gamma)\,\mathbf{n}$. ∎

By using the above lemma, we can easily obtain the first variation of the energy functional for the solid-state dewetting problem defined in (2.1).

THEOREM 2.1. *The first variation of the free energy (or shape) functional* (2.1) *used in solid-state dewetting problems with respect to a smooth vector field* $\mathbf{V}$ *can be written as*

$$\delta W(S;\mathbf{V}) = \int_S (\nabla_S\cdot\boldsymbol{\xi})\,(\mathbf{V}_0\cdot\mathbf{n})\,dS + \int_\Gamma (\mathbf{c}_\Gamma^\gamma\cdot\mathbf{n}_\Gamma + \gamma_{FS} - \gamma_{VS})(\mathbf{V}_0\cdot\mathbf{n}_\Gamma)\,d\Gamma, \tag{2.32}$$

where $\mathbf{n}_\Gamma$ *is the unit outer normal of the contact line curve* Γ *on the substrate (shown in Figure* 2.1*).*

Proof. From (2.1), we observe that the total free energy consists of two parts: the film/vapor interface energy W_{int} and the substrate energy W_{sub}. First, by using Lemma 2.1, we can directly obtain the first variation of the film/vapor interface energy W_{int} as follows:

$$\delta W_{\text{int}}(S;\mathbf{V}) = \int_S (\nabla_S\cdot\boldsymbol{\xi})\,(\mathbf{V}_0\cdot\mathbf{n})\,dS + \int_\Gamma \mathbf{V}_0\cdot\mathbf{c}_\Gamma^\gamma\,d\Gamma. \tag{2.33}$$

Here, $\mathbf{c}_\Gamma^\gamma$ is a linear combination of $\mathbf{c}_\Gamma$ and $\mathbf{n}$, which is defined on the contact line Γ. Therefore, as shown in Figure 2.1, we have

$$\mathbf{c}_\Gamma \perp \boldsymbol{\tau}_\Gamma, \quad \mathbf{n} \perp \boldsymbol{\tau}_\Gamma \quad \Rightarrow \quad \mathbf{c}_\Gamma^\gamma \perp \boldsymbol{\tau}_\Gamma. \tag{2.34}$$

For the solid-state dewetting problems studied in this paper, we assume that the contact line Γ must move along the substrate plane S_{sub}, i.e.,

$$T_\epsilon\Gamma \subset S_{\text{sub}}, \quad \mathbf{V}_0(\mathbf{x}) \,||\, S_{\text{sub}} \quad \forall\mathbf{x}\in\Gamma.$$

Therefore, for any $\mathbf{x} \in \Gamma$, $\mathbf{V}_0(\mathbf{x})$ can be decomposed into two vectors along the directions $\mathbf{n}_\Gamma(\mathbf{x})$ and $\boldsymbol{\tau}_\Gamma(\mathbf{x})$, i.e., $\mathbf{V}_0 = k_1\mathbf{n}_\Gamma + k_2\boldsymbol{\tau}_\Gamma$, where k_1 and k_2 represent the corresponding components. By making use of (2.34), we can obtain

$$\begin{aligned}\mathbf{V}_0 \cdot \mathbf{c}_\Gamma^\gamma &= (k_1\mathbf{n}_\Gamma + k_2\boldsymbol{\tau}_\Gamma) \cdot \mathbf{c}_\Gamma^\gamma = k_1(\mathbf{n}_\Gamma \cdot \mathbf{c}_\Gamma^\gamma) \\ &= (\mathbf{V}_0 \cdot \mathbf{n}_\Gamma)\,(c_\Gamma^\gamma \cdot \mathbf{n}_\Gamma) \qquad \forall \mathbf{x} \in \Gamma.\end{aligned}$$

Thus we can reformulate (2.33) as

$$\delta W_{\text{int}}(S;\mathbf{V}) = \int_S (\nabla_{_S} \cdot \boldsymbol{\xi})\ (\mathbf{V}_0 \cdot \mathbf{n})\, dS + \int_\Gamma (\mathbf{c}_\Gamma^\gamma \cdot \mathbf{n}_\Gamma)(\mathbf{V}_0 \cdot \mathbf{n}_\Gamma)\, d\Gamma. \tag{2.35}$$

On the other hand, we can rewrite the substrate energy W_{sub} as

$$W_{\text{sub}} = (\gamma_{_{FS}} - \gamma_{_{VS}})A(\Gamma) = (\gamma_{_{FS}} - \gamma_{_{VS}}) \int_{S_{_{FS}}} dS_{_{FS}}.$$

By using Proposition 2.2, and noting that the integrand φ in (2.20) is a constant and $S_{_{FS}}$ is a flat surface with a plane boundary curve Γ (i.e., $\mathcal{H} = 0$ and $\mathbf{n}_\Gamma$ is the unit conormal vector of the flat surface $S_{_{FS}}$), we directly have

$$\delta W_{\text{sub}}(S;\mathbf{V}) = (\gamma_{_{FS}} - \gamma_{_{VS}}) \int_\Gamma \mathbf{V}_0 \cdot \mathbf{n}_\Gamma\, d\Gamma. \tag{2.36}$$

By combining (2.35) and (2.36), we obtain the following conclusion:

$$\delta W(S;\mathbf{V}) = \int_S (\nabla_{_S} \cdot \boldsymbol{\xi})\ (\mathbf{V}_0 \cdot \mathbf{n})\, dS + \int_\Gamma (\mathbf{c}_\Gamma^\gamma \cdot \mathbf{n}_\Gamma + \gamma_{_{FS}} - \gamma_{_{VS}})(\mathbf{V}_0 \cdot \mathbf{n}_\Gamma)\, d\Gamma,$$

which completes the proof. ∎

REMARK 2.3. *The variational result given by* (2.32) *tells us that the rate of change of the total interfacial free energy is contributed from the two parts: one part results from the change of the interface S, and it is proportional to the weighted mean curvature (i.e., $\nabla_{_S} \cdot \boldsymbol{\xi}$)* [45] *and the rate of change of the volume (i.e., $\mathbf{V}_0 \cdot \mathbf{n}\, dS$, the normal velocity times the surface area element); the other part comes from the change of the contact line Γ.*

REMARK 2.4. *In the two-dimensional case, the variational result given by* (2.32) *in Theorem* 2.1 *will reduce to the variational result presented in* [21].

REMARK 2.5. *When the substrate is curved in 3D, the variational result given by* (2.32) *in Theorem* 2.1 *is still valid. We can perform discussions similar to those in* [19] *for curved substrates in 2D.*

3. Equilibrium shapes. The equilibrium shape of the solid-state dewetting problem can be stated as follows [5, 20]:

$$\min_\Omega W := W(S) = \int_S \gamma(\mathbf{n})\, dS + (\gamma_{_{FS}} - \gamma_{_{VS}})A(\Gamma) \quad \text{s.t.} \quad |\Omega| = \text{C}, \tag{3.1}$$

where $C > 0$ is a prescribed constant representing the total volume of the dewetted particle, and Ω represents the domain (or the particle) enclosed by the interface S and the substrate plane S_{sub}.

The Lagrangian for the above optimization problem can be defined as

$$L(S,\lambda) = \int_S \gamma(\mathbf{n})\, dS + (\gamma_{FS} - \gamma_{VS})A(\Gamma) - \lambda(|\Omega| - C), \tag{3.2}$$

with λ representing the Lagrange multiplier. The first variation of the total volume term can be obtained by simply choosing the integrand $\psi(\mathbf{x}) \equiv 1$ for all $\mathbf{x} \in \Omega$ in (2.18) by Proposition 2.1. Therefore, by combining with (2.32), the first variation of the Lagrangian with respect to a smooth vector field $\mathbf{V}$ can be given as

$$\delta L(S,\lambda;\mathbf{V}) = \int_S (\nabla_S \cdot \boldsymbol{\xi} - \lambda)(\mathbf{V}_0 \cdot \mathbf{n})\, dS + \int_\Gamma (\mathbf{c}_\Gamma^\gamma \cdot \mathbf{n}_\Gamma + \gamma_{FS} - \gamma_{VS})(\mathbf{V}_0 \cdot \mathbf{n}_\Gamma)\, d\Gamma. \tag{3.3}$$

Based on the above first variation, we have the following theorem, which yields the necessary conditions for the equilibrium shape of the solid-state dewetting problem.

THEOREM 3.1. *Assume that a two-dimensional manifold S_e with smooth boundary Γ_e is the equilibrium shape of the solid-state dewetting problem* (3.1)*; then the following conditions must be satisfied:*

$$\nabla_{S_e} \cdot \boldsymbol{\xi} = \lambda \quad \text{on } S_e, \tag{3.4a}$$

$$\mathbf{c}_\Gamma^\gamma \cdot \mathbf{n}_\Gamma + \gamma_{FS} - \gamma_{VS} = 0 \quad \text{on } \Gamma_e, \tag{3.4b}$$

where the constant λ is determined by the prescribed total volume, i.e., the constant C.

Proof. If S_e is the equilibrium shape, then (3.3) must vanish at $S = S_e$ for any smooth vector field $\mathbf{V}$. Therefore, we immediately obtain the above two necessary conditions. ∎

For isotropic surface energy, i.e., $\gamma(\mathbf{n}) \equiv 1$ (scaled by a constant γ_0), we have $\boldsymbol{\xi} = \mathbf{n}$ and $\mathbf{c}_\Gamma^\gamma = \mathbf{c}_\Gamma$. By simple calculations, (3.4a) will reduce to the condition of constant mean curvature. Denote Γ_e as the boundary of S_e. For arbitrary $\mathbf{x} \in \Gamma_e$, let $\theta_i(\mathbf{x})$ represent the equilibrium contact angle at boundary point $\mathbf{x}$. Then, (3.4b) will reduce to

$$\cos\theta_i(\mathbf{x}) = \sigma \qquad \forall \mathbf{x} \in \Gamma_e, \tag{3.5}$$

where the (dimensionless) material constant $\sigma := \frac{\gamma_{VS} - \gamma_{FS}}{\gamma_0} = \cos\theta_i$, and it is the well-known isotropic Young equation [57].

Condition (3.4b) can be regarded as the Young equation for anisotropic surface energy $\gamma(\mathbf{n})$ in 3D. For the anisotropic case, we can write the surface energy density in terms of the spherical coordinate, i.e., $\gamma_{FV} = \gamma(\theta,\phi)$ (scaled by a constant γ_0). Therefore, the Cahn–Hoffman $\boldsymbol{\xi}$-vector can be decomposed into the following three components (as shown in Figure 3.1(b)):

$$\boldsymbol{\xi}(\mathbf{n}) = \nabla\hat{\gamma}(\mathbf{n}) = \gamma(\theta,\phi)\mathbf{n} + \frac{\partial\gamma(\theta,\phi)}{\partial\theta}\boldsymbol{\tau}_\theta + \frac{1}{\sin\theta}\frac{\partial\gamma(\theta,\phi)}{\partial\phi}\boldsymbol{\tau}_\phi, \tag{3.6}$$

where in these expressions,

$$\mathbf{n} = (\sin\theta\cos\phi, \sin\theta\sin\phi, \cos\theta)^T,$$
$$\boldsymbol{\tau}_\theta = (\cos\theta\cos\phi, \cos\theta\sin\phi, -\sin\theta)^T,$$
$$\boldsymbol{\tau}_\phi = (-\sin\phi, \cos\phi, 0)^T.$$

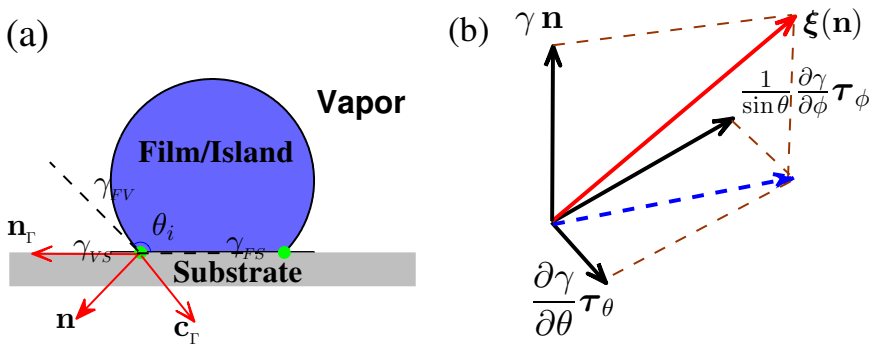

FIG. 3.1. (a) *The cross-section profile of the equilibrium shape associated with several vectors at the contact line* Γ*, where* θ_i *is the equilibrium contact angle;* (b) *the three components of the Cahn–Hoffman* $\boldsymbol{\xi}$*-vector in the spherical coordinate system.*

We obtain that the following expressions hold:

$$\boldsymbol{\xi}\cdot\mathbf{n}=\gamma(\theta,\phi),\qquad \mathbf{c}_\Gamma\cdot\mathbf{n}_\Gamma=\cos\theta(\mathbf{x}),$$
$$\boldsymbol{\xi}\cdot\mathbf{c}_\Gamma=\frac{\partial\gamma(\theta,\phi)}{\partial\theta},\qquad \mathbf{n}\cdot\mathbf{n}_\Gamma=\sin\theta(\mathbf{x}).$$

Therefore, we can rewrite (3.4b) as

$$\gamma(\theta,\phi)\cos\theta(\mathbf{x})-\frac{\partial\gamma(\theta,\phi)}{\partial\theta}\sin\theta(\mathbf{x})-\sigma=0\qquad\forall\mathbf{x}\in\Gamma_e, \tag{3.9}$$

which is consistent with the anisotropic Young equation discussed for the solid-state dewetting problem in 2D [5, 48].

If $\mathbf{X}:=\mathbf{X}(\theta,\phi)$ represents the position vector of a surface, we have $\nabla_{_S}\cdot\mathbf{X}=2$ by using Definition 2.1. Therefore, if we use the $\boldsymbol{\xi}$-plot to represent the position vector of the equilibrium shape, then the necessary condition (3.4a) will be automatically satisfied. On the one hand, this is the reason why the $\boldsymbol{\xi}$-plot can yield equilibrium shapes for a free-standing solid particle (as shown in Figure 1.1). Furthermore, based on the recent work for the generalized Winterbottom construction [5, 50], we can construct its analytical expression for the equilibrium shape which can also satisfy the contact angle condition (3.4b). First, we define a domain of definition $U_{_\phi}$ for θ under a fixed value ϕ as

$$U_{_\phi}:=\left\{\theta\Big|\gamma(\theta,\phi)\cos\theta-\frac{\partial\gamma(\theta,\phi)}{\partial\theta}\sin\theta-\sigma\geq 0,\quad \theta\in[0,\pi]\right\}, \tag{3.10}$$

where $\sigma=\frac{\gamma_{VS}-\gamma_{FS}}{\gamma_0}$. Based on Theorem 3.1, we can explicitly build its equilibrium shape in the parametric formula as $S_e(\theta,\phi):=\mathbf{X}(\theta,\phi)=(x(\theta,\phi),y(\theta,\phi),z(\theta,\phi))^T$,

$$\begin{cases} x(\theta,\phi)=\lambda\big[\gamma(\theta,\phi)\sin\theta\cos\phi+\frac{\partial\gamma(\theta,\phi)}{\partial\theta}\cos\theta\cos\phi-\frac{1}{\sin\theta}\frac{\partial\gamma(\theta,\phi)}{\partial\phi}\sin\phi\big],\\ y(\theta,\phi)=\lambda\big[\gamma(\theta,\phi)\sin\theta\sin\phi+\frac{\partial\gamma(\theta,\phi)}{\partial\theta}\cos\theta\sin\phi+\frac{1}{\sin\theta}\frac{\partial\gamma(\theta,\phi)}{\partial\phi}\cos\phi\big],\\ z(\theta,\phi)=\lambda\big[\gamma(\theta,\phi)\cos\theta-\frac{\partial\gamma(\theta,\phi)}{\partial\theta}\sin\theta-\sigma\big], \end{cases} \tag{3.11}$$

where $\phi\in[0,2\pi]$, $\theta\in U_{_\phi}$, and λ is the scaling constant determined by the total volume $|\Omega|$.

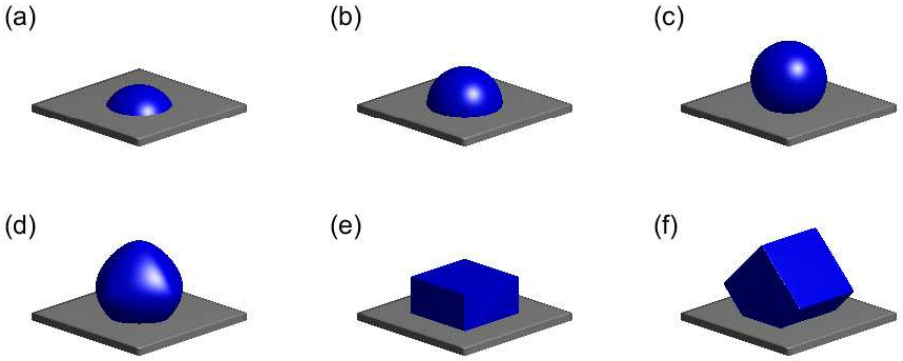

FIG. 3.2. *The equilibrium shape defined by* (3.11)*, where* (a)–(c) *is for isotropic surface energy, i.e.,* $\gamma(\mathbf{n}) \equiv 1$*, but with different material constants* $\sigma = \cos(\pi/3), \cos(\pi/2), \cos(3\pi/4)$*, respectively;* (d) $\gamma(\mathbf{n}) = 1 + 0.2(n_1^4 + n_2^4 + n_3^4)$*,* $\sigma = \cos(3\pi/4)$*;* (e) *the surface energy density is given by* (1.4)*, where* $\sigma = \cos(3\pi/4)$*,* $\varepsilon = 0.01$*;* (f) *the surface energy density is given by* $\gamma(\boldsymbol{M}_x(\pi/4)\mathbf{n})$*, where* $\gamma(\mathbf{n})$ *is defined by* (1.4) *and* $\boldsymbol{M}_x(\pi/4)$ *represents an orthogonal matrix for the rotation by an angle* $\pi/4$ *about the* x*-axis in* 3*D, using the right-hand rule, where* $\sigma = \cos(3\pi/4)$*,* $\varepsilon = 0.01$*.*

Based on the formula (3.11), the equilibrium shape under different types of surface energy anisotropies, e.g., the cubic anisotropy and regularized "cusped" anisotropy defined in (1.4), can be easily constructed. Figure 3.2(a)–(c) depicts the equilibrium shapes for isotropic surface energy with the material constant σ chosen as $\sigma = \cos(\pi/3), \cos(\pi/2), \cos(3\pi/4)$, respectively. It clearly demonstrates the effect of the material constant σ on the equilibrium shape by influencing the equilibrium contact angle via (3.5). Moreover, we also present equilibrium shapes for the cubic anisotropic surface energy, i.e., $\gamma(\mathbf{n}) = 1 + a(n_1^4 + n_2^4 + n_3^4)$, and the regularized "cusped" surface energy defined in (1.4) with $\sigma = \cos(3\pi/4)$ in Figure 3.2(d)–(e). The anisotropy for Figure 3.2(f) is chosen by a counterclockwise rotation along the x-axis by 45 degrees under the right-hand rule for the regularized "cusped" surface energy. We can observe that this rotation results in a corresponding rotation of the equilibrium shape.

4. A sharp-interface model and its properties. In this section, we propose a kinetic sharp-interface model for simulating solid-state dewetting of thin films with anisotropic surface energies, and then we show that the proposed model satisfies the mass conservation and energy dissipation.

4.1. The model. Based on (2.32) in Theorem 2.1, we can define the first variation of the total interfacial energy functional with respect to the film/vapor interface S and its boundary curve (i.e., the contact line Γ) as

$$\frac{\delta W}{\delta S} = \nabla_{_S} \cdot \boldsymbol{\xi}, \qquad \frac{\delta W}{\delta \Gamma} = \mathbf{c}_{\Gamma}^{\gamma} \cdot \mathbf{n}_{_\Gamma} + \gamma_{_{FS}} - \gamma_{_{VS}}. \tag{4.1}$$

From the Gibbs–Thomson relation [32, 44], the chemical potential can be defined as

$$\mu = \Omega_0 \frac{\delta W}{\delta S} = \Omega_0 \nabla_{_S} \cdot \boldsymbol{\xi}, \tag{4.2}$$

with Ω_0 representing the atomic volume. The normal velocity of the moving interface is controlled by surface diffusion [7, 32, 48, 20], and it can be defined as follows by Fick's laws of diffusion [4]:

$$\mathbf{J} = -\frac{D_s \nu}{k_B\, T} \nabla_{_S}\, \mu, \qquad v_n = -\Omega_0 (\nabla_{_S} \cdot \mathbf{J}) = \frac{D_s \nu \Omega_0}{k_B\, T} \nabla_{_S}^2 \mu. \tag{4.3}$$

In these expressions, $\mathbf{J}$ is the mass flux of atoms, D_s is the surface diffusivity, $k_B\, T$ is the thermal energy, ν is the number of diffusing atoms per unit area, and $\nabla_{_S}$ is the surface gradient. In addition to the surface diffusion which controls the motion of the moving interface, we still need the boundary condition for the moving contact line. Following the idea for simulating solid-state dewetting in 2D [48, 20, 19], we assume that the normal velocity of the contact line Γ is simply given by the energy gradient flow, which is determined by the time-dependent Ginzburg–Landau kinetic equations, i.e.,

$$v_{n_{_\Gamma}} = -\eta \frac{\delta W}{\delta \Gamma} = -\eta (\mathbf{c}_{_\Gamma}^{\gamma} \cdot \mathbf{n}_{_\Gamma} + \gamma_{_{FS}} - \gamma_{_{VS}}), \tag{4.4}$$

with $0 < \eta < \infty$ denoting the contact line mobility, which can be thought of as a reciprocal of a constant friction coefficient. For the physical explanation behind this approach, we refer to the recent paper [48].

We choose the characteristic length scale and characteristic surface energy scale as h_0 and γ_0, respectively, and the time scale as $\frac{h_0^4}{B\gamma_0}$, with $B = \frac{D_s \nu \Omega_0^2}{k_B\, T}$, and the contact line mobility is scaled by $\frac{B}{h_0^3}$. Let $\mathbf{X}(\cdot, t) = (x(\cdot, t), y(\cdot, t), z(\cdot, t))^T$ be a local parameterization of the moving film/vapor interface S; then we can obtain a dimensionless kinetic sharp-interface model for the solid-state dewetting of thin film via the following Cahn–Hoffman $\boldsymbol{\xi}$-vector formulation as

$$\partial_t \mathbf{X} = \Delta_{_S} \mu\, \mathbf{n}, \qquad t > 0, \tag{4.5}$$

$$\mu = \nabla_{_S} \cdot \boldsymbol{\xi}, \qquad \boldsymbol{\xi}(\mathbf{n}) = \nabla \hat{\gamma}(\mathbf{p})\Big|_{\mathbf{p}=\mathbf{n}}, \tag{4.6}$$

where t is the time, $\mathbf{n}$ is the unit outer normal vector of S, and $\boldsymbol{\xi} := \boldsymbol{\xi}(\mathbf{n})$ is the Cahn–Hoffman vector (scaled by γ_0). Here, for simplicity, we still use the same notations for all the dimensionless variables.

Let $\mathbf{X}_{_\Gamma}(\cdot, t) = (x_{_\Gamma}(\cdot, t), y_{_\Gamma}(\cdot, t), z_{_\Gamma}(\cdot, t))^T$ represent a parameterization of the moving contact line $\Gamma(t)$. The initial condition is given as S_0 with boundary Γ_0 such that

$$S_0 := \mathbf{X}(\cdot, 0) = (x_0, y_0, z_0), \qquad \Gamma_0 := \mathbf{X}(\cdot, 0)\Big|_{_\Gamma}. \tag{4.7}$$

The above governing equations are subject to the following boundary conditions:

(i) contact line condition

$$z_{_\Gamma}(\cdot, t) = 0, \quad t \geq 0; \tag{4.8}$$

(ii) relaxed contact angle condition

$$\partial_t \mathbf{X}_{_\Gamma} = -\eta \Big(\mathbf{c}_{_\Gamma}^{\gamma} \cdot \mathbf{n}_{_\Gamma} - \sigma \Big) \mathbf{n}_{_\Gamma}, \qquad t \geq 0; \tag{4.9}$$

(iii) zero-mass flux condition

$$\Big(\mathbf{c}_{_\Gamma} \cdot \nabla_{_S}\, \mu \Big)\Big|_{_\Gamma} = 0, \qquad t \geq 0; \tag{4.10}$$

where η represents a (dimensionless) contact line mobility, $\mathbf{c}_\Gamma^\gamma$ is the anisotropic conormal vector which is defined as $\mathbf{c}_\Gamma^\gamma := (\boldsymbol{\xi}\cdot\mathbf{n})\,\mathbf{c}_\Gamma - (\boldsymbol{\xi}\cdot\mathbf{c}_\Gamma)\,\mathbf{n}$, $\mathbf{c}_\Gamma$ represents the conormal vector, $\mathbf{n}_\Gamma = (n_{\Gamma,1}, n_{\Gamma,2}, 0)^T$ is the outer unit normal vector of Γ on the flat substrate (cf. Figure 2.1), and $\sigma = \frac{\gamma_{VS}-\gamma_{FS}}{\gamma_0}$ is a (dimensionless) material constant.

REMARK 4.1. *For isotropic surface energy, i.e., $\gamma(\mathbf{n}) \equiv 1$, we obtain that $\boldsymbol{\xi} = \mathbf{n}$ and $\mu = \nabla_s \cdot \boldsymbol{\xi} = \nabla_s \cdot \mathbf{n} = \mathcal{H}$; for anisotropic surface energy, by Definition* 2.1 *and some calculations, we can obtain that the dimensionless chemical potential μ is the weighted mean curvature discussed in* [45].

REMARK 4.2. *The contact line condition in* (4.8) *ensures that the contact line must move along the substrate plane. Because the contact line Γ lies on the substrate (i.e., the Oxy plane), the third component of $\mathbf{n}_\Gamma$ is always zero, i.e., $n_{\Gamma,3} = 0$. As long as the initial condition satisfies $z_\Gamma(\cdot,0) = 0$, it can automatically satisfy the boundary condition* (i) *$z_\Gamma(\cdot,t) = 0$ for all $t > 0$ by using the boundary condition* (ii). *The last boundary condition* (iii) *ensures that the total volume/mass of the thin film is conserved during the evolution, i.e., no-mass flux at the moving contact line.*

REMARK 4.3. *The above governing equation is well-posed when the surface energy is isotropic or weakly anisotropic. But when the surface energy is strongly anisotropic, some missing orientations will appear on equilibrium shapes* [40, 42]*; in this case, the governing equation becomes ill-posed, and it can be regularized by adding regularization terms such that the regularized sharp-interface model is well-posed* [20, 6]. *For the analytical criteria about the classification of surface energy anisotropy in 3D, interested readers can refer to* [40].

4.2. Mass conservation and energy dissipation. In the following, we will rigorously prove that the proposed sharp-interface model satisfies the mass conservation and the total free energy dissipation during the evolution.

PROPOSITION 4.1. *Assume that $\mathbf{X}(\cdot,t)$ is the solution of the sharp-interface model, i.e.,* (4.5)–(4.6) *with boundary conditions* (4.8)–(4.10)*, and denote $S(t) := \mathbf{X}(\cdot,t)$ as the moving film/vapor interface. Then, the total volume (or mass) of the thin film, labeled as $|\Omega(t)|$, is conserved, i.e.,*

$$|\Omega(t)| \equiv |\Omega(0)|, \qquad t \geq 0. \tag{4.11}$$

Furthermore, the (dimensionless) total interfacial free energy of the system is nonincreasing during the evolution, i.e.,

$$W(t) \leq W(t_1) \leq W(0) = \int_{S(0)} \gamma(\mathbf{n})\, dS - \sigma A(\Gamma(0)), \qquad t \geq t_1 \geq 0. \tag{4.12}$$

Proof. By making use of the first variation (2.18) and simply choosing the integrand $\psi(\mathbf{x}) \equiv 1$ for all $\mathbf{x} \in \Omega$, and using the governing equation (4.5), we can calculate the time derivative of the total volume as (noting that $\mathbf{V}_0 = \partial_t \mathbf{X}$)

$$\frac{d}{dt}|\Omega(t)| = \int_{S(t)} \partial_t \mathbf{X}\cdot\mathbf{n}\, dS = \int_{S(t)} \Delta_s \mu\, dS = 0, \qquad t \geq 0, \tag{4.13}$$

where the last equality comes from the integration by parts and the zero-mass flux condition (4.10), and it indicates that the total volume/mass is conserved.

To obtain the time derivative of the (dimensionless) total free energy, by making use of Theorem 2.1 and (2.32), but replacing the perturbation variable ϵ with the time

variable t, we can immediately obtain

$$\frac{d}{dt}W(t) = \int_{S(t)} (\nabla_{_S} \cdot \boldsymbol{\xi})\,(\partial_t \mathbf{X} \cdot \mathbf{n})\,dS + \int_{\Gamma(t)} (\mathbf{c}_{_\Gamma}^{\gamma} \cdot \mathbf{n}_{_\Gamma} - \sigma)\,(\partial_t \mathbf{X}_{\Gamma} \cdot \mathbf{n}_{_\Gamma})\,d\Gamma.$$

By substituting the governing equations and the relaxed contact angle boundary condition, i.e.,

$$\mu = \nabla_{_S} \cdot \boldsymbol{\xi}, \quad \Delta_{_S}\mu = \partial_t \mathbf{X} \cdot \mathbf{n}, \quad \partial_t \mathbf{X}_{\Gamma} \cdot \mathbf{n}_{_\Gamma} = -\eta(\mathbf{c}_{_\Gamma}^{\gamma} \cdot \mathbf{n}_{_\Gamma} - \sigma), \tag{4.14}$$

into the above equation and using the integration by parts and the zero-mass flux condition, we obtain

$$\begin{aligned} \frac{d}{dt}W(t) &= \int_{S(t)} \mu\,\Delta_S\mu\,dS - \eta \int_{\Gamma(t)} (\mathbf{c}_{_\Gamma}^{\gamma} \cdot \mathbf{n}_{_\Gamma} - \sigma)^2\,d\Gamma \\ &= -\int_{S(t)} |\nabla_{_S}\mu|^2\,dS - \eta \int_{\Gamma(t)} (\mathbf{c}_{_\Gamma}^{\gamma} \cdot \mathbf{n}_{_\Gamma} - \sigma)^2\,d\Gamma \le 0, \qquad t \ge 0, \end{aligned} \tag{4.15}$$

where the constant $\eta > 0$. The last inequality immediately implies the energy dissipation. ∎

REMARK 4.4. *In the above proof, we need to calculate the time derivatives of the total volume and the total free energy. These two derivatives can be easily obtained by making use of the speed method and the first variation presented in section* 2. *In section* 2*, we consider any type of smooth perturbations. In fact, a family of evolving interface surfaces* $\{S(t)\}_{t\ge 0}$ *can be also thought of as a type of perturbations, only by replacing the perturbation variable* ϵ *with the time variable* t*. Therefore, the time derivatives can be directly obtained by using the first variation of the total volume functional and the total free energy functional.*

5. Numerical results. In this section, we perform numerical simulations for solid-state dewetting in 3D to investigate the morphological evolution of thin films in various cases. We implement the parametric finite element method (PFEM) [6, 58] for solving the proposed sharp-interface model in 3D. For the detailed introduction of numerical algorithms about the PFEM in 3D, interested readers can refer to [58].

First, we focus on the case for isotropic surface energy, i.e., $\gamma(\mathbf{n}) \equiv 1$. We start with numerical examples for an initial short cuboid island with $(4, 4, 1)$ representing its length, width, and height, respectively (as shown in Figure 5.1(a)). The computational parameter is chosen as $\sigma = \cos(5\pi/6)$. In Figure 5.1, we show several snapshots of the morphology evolution for the short cuboid towards its equilibrium shape. As time evolves, the initial sharp corners and edges along the island become smoother and smoother (see Figure 5.1(b)), and finally the island film approaches a spherical shape as its equilibrium shape (see Figure 5.1(f)).

Short cuboid island films tend to form a single spherical shape as its equilibrium which minimizes its total free energy (i.e., the minimal surface area). However, the morphological evolution for long cuboid islands could be quite different. Due to the Plateau–Rayleigh instability [26, 38, 31], long cuboid islands could pinch off and break up into a number of small isolated particles on the substrate before they approach a single spherical shape as its equilibrium. In order to investigate this phenomenon, we perform the simulation by choosing the material constant as $\sigma = \cos(3\pi/4)$ and the shape of the initial island film as a long cuboid with $(1, 12, 1)$. For the isotropic case, as can be seen in Figure 5.2, the island quickly evolves into a cylinder-like shape during

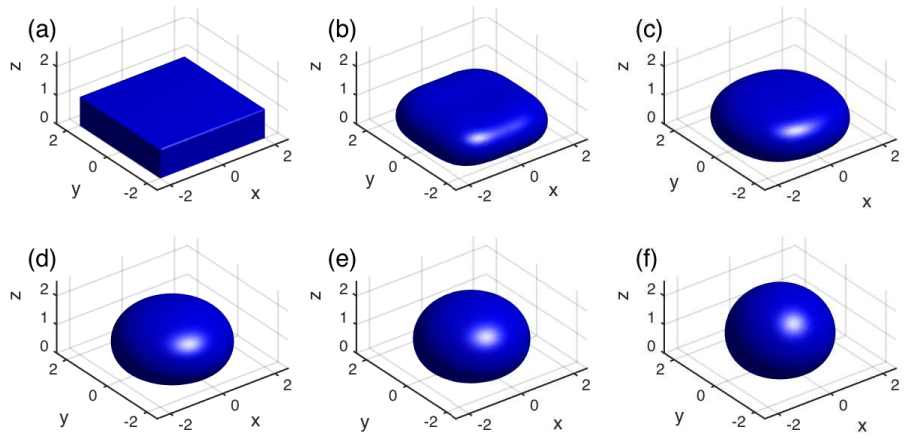

FIG. 5.1. *Several snapshots during the evolution of an initial cuboid island film with isotropic surface energy towards its equilibrium shape:* (a) $t = 0$; (b) $t = 0.1$; (c) $t = 0.2$; (d) $t = 0.5$; (e) $t = 0.7$; (f) $t = 1.4$, *where the initial shape of the thin film is chosen as a* $(4, 4, 1)$ *cuboid, and the material constant is chosen as* $\sigma = \cos(5\pi/6)$.

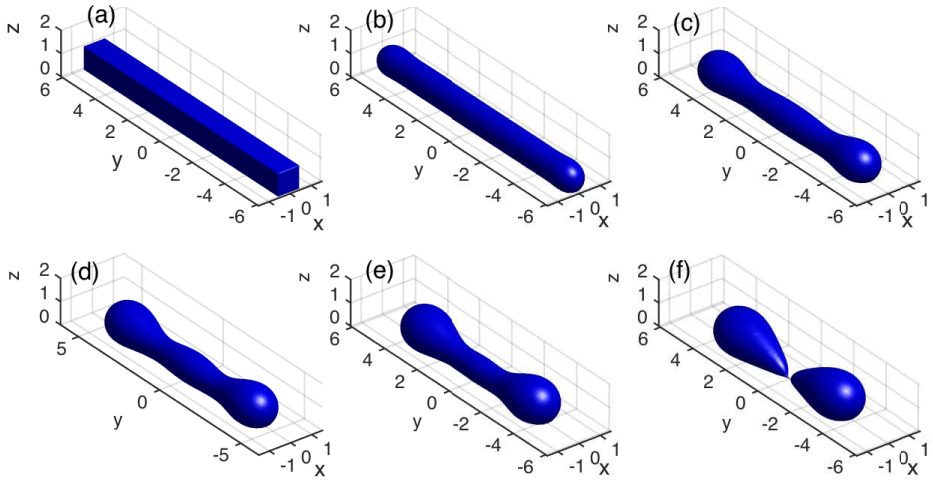

FIG. 5.2. *Several snapshots during the evolution of an initial cuboid island film with isotropic surface energy until its pinch-off time:* (a) $t = 0$; (b) $t = 0.01$; (c) $t = 0.30$; (d) $t = 0.50$; (e) $t = 0.80$; (f) $t = 1.07$, *where the initial shape is chosen as a* $(1, 12, 1)$ *cuboid, and the material constant* $\sigma = \cos(3\pi/4)$.

the evolution; then it accumulates more and more materials near the two edges, while the two necks appear and become thinner and thinner; finally, it pinches off at the neck and breaks up into two small isolated islands on the substrate. For cubic anisotropic surface energies, long cuboid islands also exhibit a pinch-off process similar to the isotropic surface energy case. We test the numerical example for an initial cuboid island with the same material constant and initial shape, as shown in Figure 5.3. From the figure, we observe that three isolated small particles finally appear, while only two small particles are finally produced by the solid-state dewetting process in

the isotropic case. This indicates that for this type of cubic anisotropic surface energy, the solid film tends to dewet more easily and quickly than in the isotropic case.

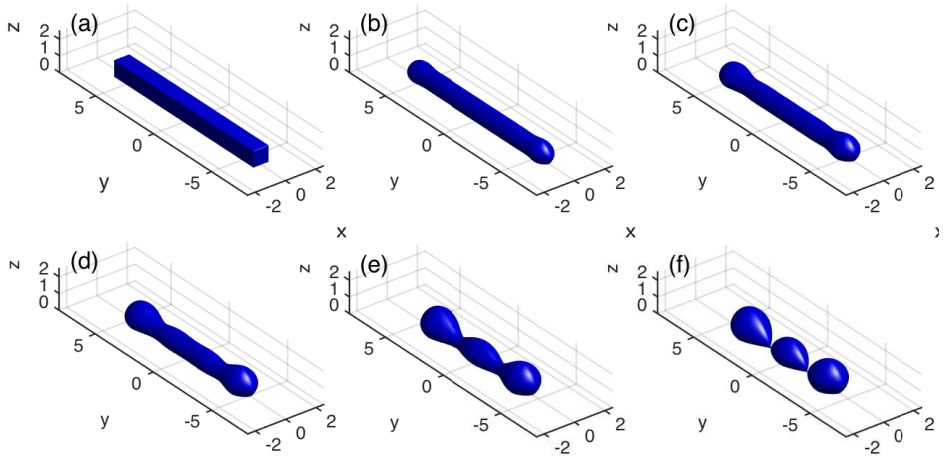

FIG. 5.3. *Several snapshots during the evolution of an initial cuboid island film with anisotropic surface energy until its pinch-off time:* (a) $t = 0$; (b) $t = 0.020$; (c) $t = 0.100$; (d) $t = 0.240$; (e) $t = 0.540$; (f) $t = 0.695$, *where the initial shape is chosen as a* $(1, 12, 1)$ *cuboid, the material constant* $\sigma = \cos(3\pi/4)$, *and the anisotropic surface energy is chosen as the cubic type, i.e.,* $\gamma(\mathbf{n}) = 1 + a(n_1^4 + n_2^4 + n_3^4)$, *with* $a = 0.25$.

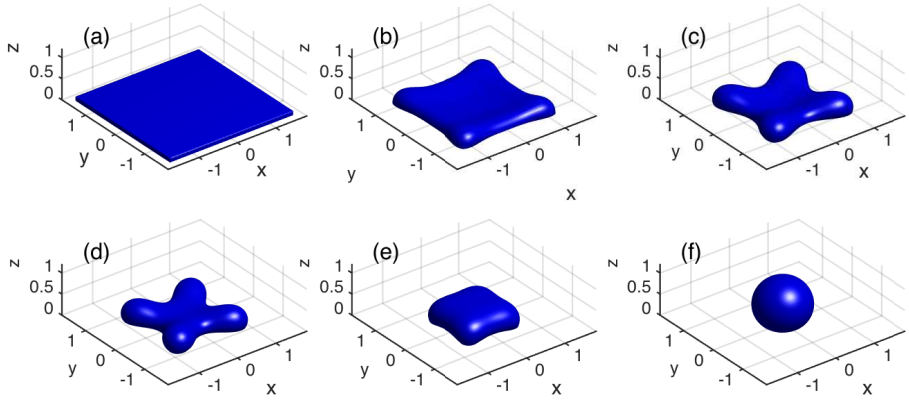

FIG. 5.4. *Several snapshots during the evolution of an initial small square island film with isotropic surface energy towards its equilibrium shape:* (a) $t = 0$; (b) $t = 0.004$; (c) $t = 0.008$; (d) $t = 0.012$; (e) $t = 0.020$; (f) $t = 0.080$, *where the initial shape is chosen as a* $(3.2, 3.2, 0.1)$ *cuboid, and the material constant* $\sigma = \cos(5\pi/6)$.

Finally, we investigate the morphological evolution of square island films with size (m, m, h) on a flat substrate. We start by simulating the evolution of an initial small square island with size $(3.2, 3.2, 0.1)$, and the material constant is chosen as $\sigma = \cos(5\pi/6)$. As can be seen in Figure 5.4, at the beginning, the square island retracts much more slowly at its four corners than at the middle points of the four edges. As time evolves, this process results in an almost cross shape (see Figure 5.4(c)–

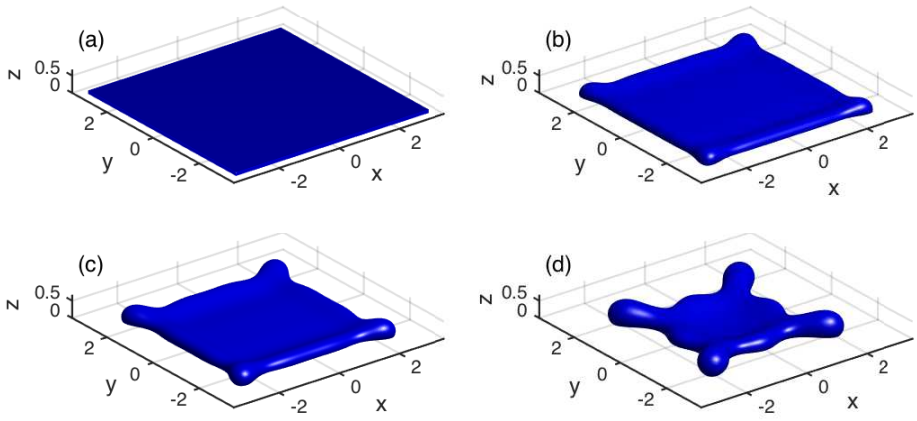

FIG. 5.5. *Several snapshots during the evolution of an initial large square island film with isotropic surface energy until its pinch-off time:* (a) $t = 0$; (b) $t = 0.005$; (c) $t = 0.010$; (d) $t = 0.031$, *where the initial shape is chosen as a* $(6.4, 6.4, 0.1)$ *cuboid, and the material constant* $\sigma = \cos(5\pi/6)$.

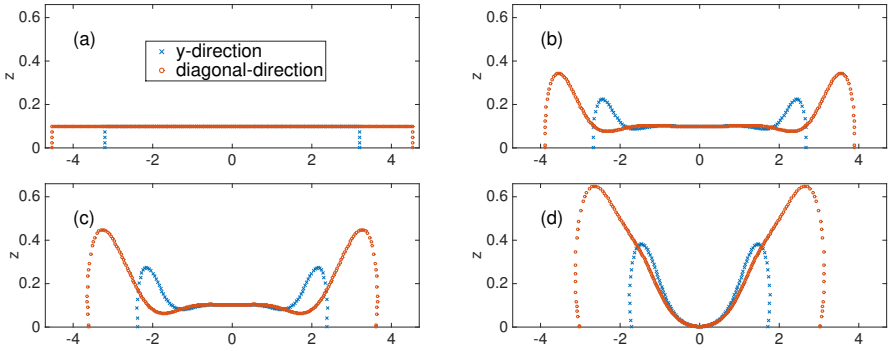

FIG. 5.6. *The cross-section profile of the island film along its y-direction and diagonal direction for the example shown in Figure* 5.5: (a) $t = 0$; (b) $t = 0.005$; (c) $t = 0.010$; (d) $t = 0.031$.

(d)). This phenomenon, known as "mass accumulation" at the corner, has been previously observed in experiments [46, 54, 56] or numerical simulations by a phase-field approach [18, 33]. Subsequently, because the length of the square island is small, these retracting corners eventually catch up with the edges; then the contact line begins to move towards a circular shape in order to approach a spherical shape as its equilibrium (see Figure 5.4(f)). During the evolution, we also observe that a valley appears at the center of the island, but finally it disappears. To observe the possible pinch-off phenomenon, we enlarge the square size and simulate the evolution of an initial large square island with size $(6.4, 6.4, 0.1)$ (shown in Figure 5.5). From the figure, we observe that the valley at the center becomes deeper and deeper, and it eventually touches the substrate and produces a hole in the center of the island. We stop the numerical simulation at the moment when there exists one new mesh point which touches the substrate. For a better illustration, in Figure 5.6, we also plot several snapshots about its cross-section profile of the island film during the evolution.

6. Conclusions. We proposed a sharp-interface model for simulating solid-state dewetting of thin films in 3D, and this model can include the effect of the surface energy anisotropy. Based on the Cahn–Hoffman $\boldsymbol{\xi}$-vector formulation and shape derivatives, we derived rigorously the first variation of the total free energy functional of the solid-state dewetting problem. From the first variation, necessary conditions for the equilibrium shape of solid-state dewetting were rigorously given in mathematics. Furthermore, a kinetic sharp-interface model was also proposed for simulating the solid-state dewetting of thin films in 3D. The governing equations described the interface evolution which is controlled by surface diffusion and contact line migration. Numerical simulations were performed by solving the proposed sharp-interface model, and numerical results reproduced the complex features in the solid thin film dewetting observed in experiments, such as edge retraction, hole formation, faceting, corner accumulation, pinch-off, and Rayleigh instability.

In this paper, we assume that the capillarity is the only driving force for solid-state dewetting, and that the effect of elasticity associated with a mismatch strain in the film layer during deposition is negligible, which is often the case for Ni films on MgO substrates and Si films on amorphous SiO_2 substrates (i.e., SOI). In the future, we can include the elastic effect into the model to study dewetting phenomena in semiconductor electronic and optoelectronic devices (such as In-GaAs/GaAs and SiGe/Si systems), especially for studying the Stranski–Krastanow (SK) and Volmer–Weber (VW) growth modes. Meanwhile, we can also study how the material microstructure affects the boundary conditions as discussed in [47].

REFERENCES

[1] D. Alpay, L. Peng, and L. D. Marks, *Are nanoparticle corners round?*, J. Phys. Chem. C, 119 (2015), pp. 21018–21023.

[2] D. Amram, L. Klinger, and E. Rabkin, *Anisotropic hole growth during solid-state dewetting of single-crystal Au–Fe thin films*, Acta Mater., 60 (2012), pp. 3047–3056.

[3] L. Armelao, D. Barreca, G. Bottaro, A. Gasparotto, S. Gross, C. Maragno, and E. Tondello, *Recent trends on nanocomposites based on Cu, Ag and Au clusters: A closer look*, Coord. Chem. Rev., 250 (2006), pp. 1294–1314.

[4] R. W. Balluffi, S. Allen, and W. C. Carter, *Kinetics of Materials*, John Wiley & Sons, New York, 2005.

[5] W. Bao, W. Jiang, D. J. Srolovitz, and Y. Wang, *Stable equilibria of anisotropic particles on substrates: A generalized Winterbottom construction*, SIAM J. Appl. Math., 77 (2017), pp. 2093–2118, https://doi.org/10.1137/16M1091599.

[6] W. Bao, W. Jiang, Y. Wang, and Q. Zhao, *A parametric finite element method for solid-state dewetting problems with anisotropic surface energies*, J. Comput. Phys., 330 (2017), pp. 380–400.

[7] J. Cahn and D. Hoffman, *A vector thermodynamics for anisotropic surfaces* II: *Curved and faceted surfaces*, Acta Metall., 22 (1974), pp. 1205–1214.

[8] J. W. Cahn and C. A. Handwerker, *Equilibrium geometries of anisotropic surfaces and interfaces*, Mater. Sci. Eng. A, 162 (1993), pp. 83–95.

[9] W. C. Carter, A. R. Roosen, J. W. Cahn, and J. E. Taylor, *Shape evolution by surface diffusion and surface attachment limited kinetics on completely faceted surfaces*, Acta Metall. Mater., 43 (1995), pp. 4309–4323.

[10] K. Deckelnick, G. Dziuk, and C. M. Elliott, *Computation of geometric partial differential equations and mean curvature flow*, Acta Numer., 14 (2005), pp. 139–232.

[11] G. Doğan and R. H. Nochetto, *First variation of the general curvature-dependent surface energy*, ESAIM Math. Model. Numer. Anal., 46 (2012), pp. 59–79.

[12] E. Dornel, J. Barbe, F. De Crécy, G. Lacolle, and J. Eymery, *Surface diffusion dewetting of thin solid films: Numerical method and application to Si/SiO_2*, Phys. Rev. B, 73 (2006), 115427.

[13] P. Du, M. Khenner, and H. Wong, *A tangent-plane marker-particle method for the computation of three-dimensional solid surfaces evolving by surface diffusion on a substrate*, J.

Comput. Phys., 229 (2010), pp. 813–827.
[14] G. Dziuk and C. M. Elliott, *Finite element methods for surface PDEs*, Acta Numer., 22 (2013), pp. 289–396.
[15] M. Dziwnik, A. Münch, and B. Wagner, *An anisotropic phase-field model for solid-state dewetting and its sharp-interface limit*, Nonlinearity, 30 (2017), pp. 1465–1496.
[16] M. Hintermüller and W. Ring, *A second order shape optimization approach for image segmentation*, SIAM J. Appl. Math., 64 (2003), pp. 442–467, https://doi.org/10.1137/S0036139902403901.
[17] D. W. Hoffman and J. W. Cahn, *A vector thermodynamics for anisotropic surfaces*: I. *Fundamentals and application to plane surface junctions*, Surf. Sci., 31 (1972), pp. 368–388.
[18] W. Jiang, W. Bao, C. V. Thompson, and D. J. Srolovitz, *Phase field approach for simulating solid-state dewetting problems*, Acta Mater., 60 (2012), pp. 5578–5592.
[19] W. Jiang, Y. Wang, D. J. Srolovitz, and W. Bao, *Solid-state dewetting on curved substrates*, Phys. Rev. Mater., 2 (2018), 113401.
[20] W. Jiang, Y. Wang, Q. Zhao, D. J. Srolovitz, and W. Bao, *Solid-state dewetting and island morphologies in strongly anisotropic materials*, Scripta Mater., 115 (2016), pp. 123–127.
[21] W. Jiang and Q. Zhao, *Sharp-interface approach for simulating solid-state dewetting in two dimensions: A Cahn-Hoffman $\boldsymbol{\xi}$-vector formulation*, Phys. D, 390 (2019), pp. 69–83.
[22] W. Jiang, Q. Zhao, T. Qian, D. J. Srolovitz, and W. Bao, *Application of Onsager's variational principle to the dynamics of a solid toroidal island on a substrate*, Acta Mater., 163 (2019), pp. 154–160.
[23] E. Jiran and C. Thompson, *Capillary instabilities in thin films*, J. Electron. Mater., 19 (1990), pp. 1153–1160.
[24] R. Kaischew, *Equilibrium shape and work of formation of crystalline nuclei on a foreign substrate*, Commun. Bulg. Acad. Sci., 1 (1950), pp. 100–136 (in Bulgarian).
[25] W. Kan and H. Wong, *Fingering instability of a retracting solid film edge*, J. Appl. Phys., 97 (2005), 043515.
[26] G. H. Kim and C. V. Thompson, *Effect of surface energy anisotropy on Rayleigh-like solid-state dewetting and nanowire stability*, Acta Mater., 84 (2015), pp. 190–201.
[27] G. H. Kim, R. V. Zucker, J. Ye, W. C. Carter, and C. V. Thompson, *Quantitative analysis of anisotropic edge retraction by solid-state dewetting of thin single crystal films*, J. Appl. Phys., 113 (2013), 043512.
[28] M. D. Korzec, M. Roczen, M. Schade, B. Wagner, and B. Rech, *Equilibrium shapes of polycrystalline silicon nanodots*, J. Appl. Phys., 115 (2014), 074304.
[29] O. Kovalenko, S. Szabó, L. Klinger, and E. Rabkin, *Solid state dewetting of polycrystalline Mo film on sapphire*, Acta Mater., 139 (2017), pp. 51–61.
[30] F. Leroy, Ł. Borowik, F. Cheynis, Y. Almadori, S. Curiotto, M. Trautmann, J. Barbé, and P. Müller, *How to control solid state dewetting: A short review*, Surf. Sci. Rep., 71 (2016), pp. 391–409.
[31] M. S. McCallum, P. W. Voorhees, M. J. Miksis, S. H. Davis, and H. Wong, *Capillary instabilities in solid thin films: Lines*, J. Appl. Phys., 79 (1996), pp. 7604–7611.
[32] W. W. Mullins, *Theory of thermal grooving*, J. Appl. Phys., 28 (1957), pp. 333–339.
[33] M. Naffouti, R. Backofen, M. Salvalaglio, T. Bottein, M. Lodari, A. Voigt, T. David, A. Benkouider, I. Fraj, L. Favre, A. Ronda, I. Berbezier, D. Grosso, M. Abbarchi, and M. Bollani, *Complex dewetting scenarios of ultrathin silicon films for large-scale nanoarchitectures*, Sci. Adv., 3 (2017), eaao1472.
[34] D. Peng, S. Osher, B. Merriman, and H.-K. Zhao, *The geometry of Wulff crystal shapes and its relations with Riemann problems*, in Nonlinear Partial Differential Equations, AMS, Providence, RI, 1998, pp. 251–303.
[35] O. Pierre-Louis, A. Chame, and Y. Saito, *Dewetting of ultrathin solid films*, Phys. Rev. Lett., 103 (2009), 195501.
[36] E. Rabkin, D. Amram, and E. Alster, *Solid state dewetting and stress relaxation in a thin single crystalline Ni film on sapphire*, Acta Mater., 74 (2014), pp. 30–38.
[37] S. Randolph, J. Fowlkes, A. Melechko, K. Klein, H. Meyer III, M. Simpson, and P. Rack, *Controlling thin film structure for the dewetting of catalyst nanoparticle arrays for subsequent carbon nanofiber growth*, Nanotechnology, 18 (2007), 465304.
[38] L. Rayleigh, *On the instability of jets*, Proc. Lond. Math. Soc., 1 (1878), pp. 4–13.
[39] V. Schmidt, J. V. Wittemann, S. Senz, and U. Gösele, *Silicon nanowires: A review on aspects of their growth and their electrical properties*, Adv. Mater., 21 (2009), pp. 2681–2702.
[40] R. F. Sekerka, *Analytical criteria for missing orientations on three-dimensional equilibrium*

shapes, J. Crystal Growth, 275 (2005), pp. 77–82.
[41] J. Sokołowski and J. Zolesio, *Introduction to Shape Optimization: Shape Sensitivity Analysis*, Springer-Verlag, Berlin, 1992.
[42] B. J. Spencer, *Asymptotic solutions for the equilibrium crystal shape with small corner energy regularization*, Phys. Rev. E (3), 69 (2004), 011603.
[43] D. J. Srolovitz and S. A. Safran, *Capillary instabilities in thin films*: II. *Kinetics*, J. Appl. Phys., 60 (1986), pp. 255–260.
[44] A. P. Sutton and R. W. Balluffi, *Interfaces in Crystalline Materials*, Clarendon Press, Oxford, UK, 1995.
[45] J. E. Taylor, II–*mean curvature and weighted mean curvature*, Acta Metall. Mater., 40 (1992), pp. 1475–1485.
[46] C. V. Thompson, *Solid-state dewetting of thin films*, Annu. Rev. Mater. Res., 42 (2012), pp. 399–434.
[47] A. K. Tripathi and O. Pierre-Louis, *Triple-line kinetics for solid films*, Phys. Rev. E (3), 97 (2018), 022801.
[48] Y. Wang, W. Jiang, W. Bao, and D. J. Srolovitz, *Sharp interface model for solid-state dewetting problems with weakly anisotropic surface energies*, Phys. Rev. B, 91 (2015), 045303.
[49] A. A. Wheeler and G. B. McFadden, *A $\boldsymbol{\xi}$-vector of anisotropic phase-field models: 3D asymptotics*, European J. Appl. Math., 7 (1996), pp. 367–381.
[50] W. Winterbottom, *Equilibrium shape of a small particle in contact with a foreign substrate*, Acta Metall., 15 (1967), pp. 303–310.
[51] H. Wong, P. Voorhees, M. Miksis, and S. Davis, *Periodic mass shedding of a retracting solid film step*, Acta Mater., 48 (2000), pp. 1719–1728.
[52] G. Wulff, *Zur frage der geschwindigkeit des wachstums und der auflösung der krystallflächen*, Z. Kristallogr, 34 (1901), pp. 449–530.
[53] J. Ye and C. V. Thompson, *Mechanisms of complex morphological evolution during solid-state dewetting of single-crystal nickel thin films*, Appl. Phys. Lett., 97 (2010), 071904.
[54] J. Ye and C. V. Thompson, *Regular pattern formation through the retraction and pinch-off of edges during solid-state dewetting of patterned single crystal films*, Phys. Rev. B, 82 (2010), 193408.
[55] J. Ye and C. V. Thompson, *Anisotropic edge retraction and hole growth during solid-state dewetting of single crystal nickel thin films*, Acta Mater., 59 (2011), pp. 582–589.
[56] J. Ye and C. V. Thompson, *Templated solid-state dewetting to controllably produce complex patterns*, Adv. Mater., 23 (2011), pp. 1567–1571.
[57] T. Young, *An essay on the cohesion of fluids*, Philos. Trans. R. Soc. London, 95 (1805), pp. 65–87.
[58] Q. Zhao, W. Jiang, and W. Bao, *A parametric finite element method for solid-state dewetting problems in three dimensions*, SIAM J. Sci. Comput., 42 (2020), pp. B327–B352, https://doi.org/10.1137/19M1281666.
[59] R. V. Zucker, G. H. Kim, W. C. Carter, and C. V. Thompson, *A model for solid-state dewetting of a fully-faceted thin film*, C. R. Physique, 14 (2013), pp. 564–577.